

#### ARTICLE OPEN



# Low-temperature dielectric anomaly arising from electronic phase separation at the Mott insulator-metal transition

A. Pustogow ( $^{1,2,8}$ ), R. Rösslhuber ( $^{1,8}$ ), Y. Tan<sup>3,8</sup>, E. Uykur<sup>1</sup>, A. Böhme<sup>1</sup>, M. Wenzel<sup>1</sup>, Y. Saito<sup>1,4</sup>, A. Löhle<sup>1</sup>, R. Hübner ( $^{1,5}$ ), A. Kawamoto<sup>4</sup>, J. A. Schlueter<sup>6,7</sup>, V. Dobrosavljević ( $^{1,6}$ ) and M. Dressel ( $^{1,6}$ )

Coulomb repulsion among conduction electrons in solids hinders their motion and leads to a rise in resistivity. A regime of electronic phase separation is expected at the first-order phase transition between a correlated metal and a paramagnetic Mott insulator, but remains unexplored experimentally as well as theoretically nearby T = 0. We approach this issue by assessing the complex permittivity via dielectric spectroscopy, which provides vivid mapping of the Mott transition and deep insight into its microscopic nature. Our experiments utilizing both physical pressure and chemical substitution consistently reveal a strong enhancement of the quasi-static dielectric constant  $\varepsilon_1$  when correlations are tuned through the critical value. All experimental trends are captured by dynamical mean-field theory of the single-band Hubbard model supplemented by percolation theory. Our findings suggest a similar 'dielectric catastrophe' in many other correlated materials and explain previous observations that were assigned to multiferroicity or ferroelectricity.

npj Quantum Materials (2021)6:9; https://doi.org/10.1038/s41535-020-00307-0

#### INTRODUCTION

Insulator-metal transitions (IMTs) remain one of the unresolved science problems of condensed-matter physics, which are rather general and of fundamental importance. Especially intriguing are those IMTs not associated with static symmetry changes, where paradigms for conventional phase transitions provide little guidance. Early examples of such behavior are found in certain disorder-driven IMTs<sup>1</sup>. In recent years, IMTs with no symmetry breaking were also identified around the Mott transition<sup>2–5</sup>, which bears close connection to exotic states of strongly correlated electron matter, such as unconventional superconductivity and quantum spin liquids (QSLs). From a theoretical point of view, the single-band Hubbard model is well understood<sup>6,7</sup>, and is found to be in excellent agreement with experiments<sup>5,8–10</sup>. While commonly concealed by antiferromagnetism, recent development in the field of organic QSLs enabled investigation of the lowtemperature Mott IMT in absence of magnetic order<sup>11-14</sup>, revealing finite-frequency precursors of the metal already on the insulating side 15.

At half filling, the Mott insulator and the correlated metal converge at the critical endpoint  $T_{\rm crit}$  (Fig. 1). The former is bounded by a quantum-critical region along the quantum Widom line (QWL)<sup>5,15-18</sup>. On the metallic side, resistivity maxima at the Brinkman-Rice temperature  $T_{\rm BR}$  signal the thermal destruction of resilient quasiparticles<sup>19,20</sup> and the crossover to semiconducting transport. Below  $T_{\rm critr}$  the IMT is of first order and comprises an insulator-metal coexistence regime<sup>6,16,17</sup>. Figure 1 displays the phase diagram of genuine Mott systems at half filling without magnetic order<sup>15</sup>, as realized in triangular-lattice organic compounds subject to strong geometrical frustration<sup>5,11-14,21</sup>. Note, many oxides are charge-transfer insulators<sup>22</sup> and involve a pronounced coupling of the IMT to the lattice<sup>10,23</sup>, whereas the

molecular materials studied here are ideal model systems to elucidate single-band Mott insulators without significant structural modifications at the transition to the metallic state. It is currently debated whether the electrodynamics of the genuine Mott IMT is dominated by closing of the Mott gap or by spatial inhomogeneity, fueled by recent low-temperature transport studies<sup>14</sup>.

Although the high-quality crystals we investigate typically feature uniform insulating and metallic phases, the situation is more subtle within the IMT phase-coexistence region at  $T < T_{crit}$ . Similarly to most other systems close to first-order phase transitions, here one generally expects spatial segregation into domains of the coexisting phases, and the associated metastability and hysteresis phenomena. Seminal transport and susceptibility experiments indeed found a pronounced hysteresis in the Mott systems  $V_2O_3$  and  $\kappa$ -(BEDT-TTF)<sub>2</sub>Cu[N(CN)<sub>2</sub>]Cl featuring magnetically-ordered ground states<sup>8,9,24</sup>. Unfortunately, analogue measurements with continuous pressure tuning are not feasible on QSL compounds, such as κ-(BEDT-TTF)2Cu2(CN)3, due to the low temperatures (T < 20 K) and high pressures (p > 1 kbar) required to cross the first-order IMT. Alternative methods are, therefore, required in these systems in order to reveal and mapout regimes where such inhomogeneous electronic states arise. While different microscopic mechanisms can, in principle, contribute to stabilizing such inhomogeneous phase separation (see discussion below), in electronic systems it proves to dramatically modify the electrodynamic response leading to robust percolation phenomena that depend only weakly on the system-dependent details. This observation, as we shall demonstrate below, allows us to clearly recognize and understand the regime dominated by phase coexistence, resolving much of the controversy associated with the nature of the Mott point in QSL compounds.

<sup>&</sup>lt;sup>1</sup>1. Physikalisches Institut, Universität Stuttgart, 70569 Stuttgart, Germany. <sup>2</sup>Department of Physics and Astronomy, UCLA, Los Angeles, CA 90095, USA. <sup>3</sup>Department of Physics and National High Magnetic Field Laboratory, Florida State University, Tallahassee, Florida 32306, USA. <sup>4</sup>Department of Physics, Hokkaido University, Sapporo 060-0810, Japan. <sup>5</sup>Inst. für Klinische Radiologie und Nuklearmedizin, Universität Heidelberg, Mannheim, Germany. <sup>6</sup>Material Science Division, Argonne National Laboratory, Argonne, IL 60439-4831, USA. <sup>7</sup>Division of Materials Research, National Science Foundation, Alexandria, VA 22314, USA. <sup>8</sup>These authors contributed equally. A. Pustogow, R. Rösslhuber, Y. Tan. <sup>©</sup>email: andrej.pustogow@pi1.physik.uni-stuttgart.de; vlad@magnet.fsu.edu; dressel@pi1.physik.uni-stuttgart.de





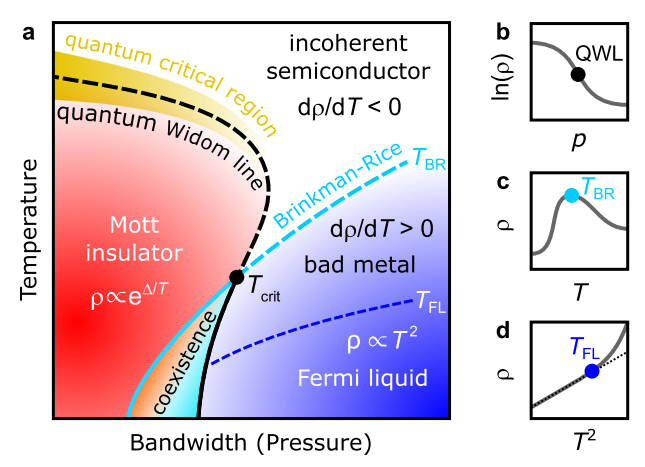


Fig. 1 Electronic transport regimes around the *genuine* Mott insulator-metal transition at half filling. a Tuning the bandwidth W, for instance by chemical or physical pressure, transforms a Mott insulator to a correlated metal. Dynamical mean-field theory predicts a first-order transition with phase coexistence (delimited by solid lines) up to the critical endpoint<sup>6</sup>, and a quantum-critical regime associated with the quantum Widom line (QWL, dashed black line) above  $T_{\rm crit}$ . The metallic state is confined by the Brinkman-Rice temperature  $T_{\rm BR}$  (dashed cyan) at  $T > T_{\rm crit}$ , the coherent Fermi-liquid regime by  $T_{\rm FL}$  (dashed blue). When interactions U are comparable to W, and  $T \gg T_{\rm crit}$ , semiconducting behavior prevails; neither a gap nor a quasiparticle peak are stabilized.  ${\bf b}-{\bf d}$  Resistivity signatures of the crossovers in dc transport.  ${\bf b}$  The steepest slope of  ${\bf ln}$   $\{\rho({\bf p})\}$  indicates the crossing of the QWL upon a pressure sweep.  ${\bf c}$   $T_{\rm BR}$  indicates the transition from an insulating  $(d\rho/dT < 0)$  to a metallic  $(d\rho/dT > 0)$  temperature dependence.  ${\bf d}$  The  $\rho(T) \propto T^2$  behavior extends up to  $T_{\rm FL}$ .

A more direct insight into the coexistence region was provided by spatially resolved optical spectroscopy<sup>25</sup>. The most compelling results came from near-field infrared experiments on VO<sub>2</sub> by Basov and collaborators<sup>26</sup> where a spatial separation of metallic and insulating regions upon heating could be visualized, in accord with X-ray studies  $^{10,27}$ ; the range of hysteresis in  $\rho(T)$  coincides with the observed phase coexistence. Although recent developments in cryogenic near-field instrumentation are rather promising<sup>28–30</sup>, they fall short of covering the regime  $T < T_{crit} \approx 15$  K required here and do not allow for pressure tuning. For this reason, we suggest dielectric spectroscopy as a powerful bulksensitive method in order to unravel the coexistence regime, distinguish the individual phases and obtain a deeper understanding of the dynamics around the IMT. The complex conductivity  $\sigma_1 + i\sigma_2$  not only reveals the closing of the Mott gap but yields insight into the growth of metallic regions and the formation of quasiparticles as correlation effects decrease.

Here we tackle the fundamental question whether electrodynamic response around the Mott IMT is overwhelmed by the gradual decrease of the Mott-Hubbard gap within a homogeneous insulating phase, or whether the effects of phase coexistence dominate. Furthermore, is it possible to distinguish on the metallic side between the coherent (quasiparticle) low-T regime and incoherent transport at high-T? To answer these questions, we present temperature- and frequency-dependent dielectric measurements on a genuine Mott compound that is bandwidth-tuned across its first-order IMT. In addition to hydrostatic pressure we developed an innovative approach of chemically substituting the organic donor molecules. The experimental findings are complemented by dynamical mean-field theory (DMFT) calculations, incorporating spatial inhomogeneities in a hybrid approach. We conclude that electronic phase segregation plays a crucial role, leading to percolative phenomena due to the separation of insulating and metallic regions, also allowing clear and precise mapping of different dynamical regimes around the IMT.

#### **RESULTS**

#### Mott transition through pressure and chemical substitution

We have chosen  $\kappa$ -(BEDT-TTF)<sub>2</sub>Cu<sub>2</sub>(CN)<sub>3</sub> single crystals for our investigations because this paradigmatic QSL candidate is well characterized by electric, optical and magnetic measurements<sup>3,14,15,21,31,32</sup>. Although the dimerized charge-transfer salt possesses a half-filled conduction band, strong electronic interaction  $U \approx 250$  meV stabilizes a Mott-insulating state below the QWL  $(T_{OWI} \approx 185 \text{ K at ambient pressure}^{5,15})$  with no magnetic order observed down to mK temperatures<sup>3</sup>. The effective correlation strength U/W can be reduced by increasing the bandwidth W; for pressure p > 1.4 kbar the metallic state is reached at low temperatures, with  $T_{crit} \approx 15-20$  K. In addition, we exploited an alternative route of partially replacing the S atoms of the donor molecules by Se, where more extended orbitals lead to larger bandwidth (see sketches in Fig. 2h, k). The substitutional series  $\kappa$ -[(BEDT-TTF)<sub>1-x</sub>(BEDT-STF)<sub>x</sub>]<sub>2</sub>Cu<sub>2</sub>(CN)<sub>3</sub> (0  $\leq$  x  $\leq$  1, abbreviated  $\kappa$ -STF<sub>x</sub>) spans the interval ranging from a Mott insulator to a Fermiliquid metal. Details on the sample characterization and experimental methods are given in Supplementary Note 1. Here we focus on the out-of-plane dielectric response measured from f=7.5 kHz to 5 MHz down to T=5 K. Both physical pressure and BEDT-STF substitution allow us to monitor the permittivity while shifting the system across the first-order IMT.

#### Metal-insulator transition mapped by dielectric permittivity

Figure 2 displays the temperature-dependent conductivity and permittivity data of  $\kappa$ -(BEDT-TTF) $_2$ Cu $_2$ (CN) $_3$  when p rises (a–e) and x increases in  $\kappa$ -STF $_x$  (f–j). The insulating state (p < 1.4 kbar, x < 0.1), characterized by d $\sigma_1/dT > 0$ , generally features small positive  $\varepsilon_1 \approx 10$ . The relaxor-like response previously observed in the parent compound below 50 K has been subject of debate  $^{33,34}$ . The metallic state (p > 3 kbar, x > 0.2) is defined by d $\sigma_1/dT$  < 0 and, concomitantly,  $\varepsilon_1$  < 0 that becomes very large at low T as itinerant electrons increasingly screen. Comparison of the results in Fig. 2j with optical data measured on the same substitution yields fair agreement of the metallic values  $\varepsilon_1$  < 0 (see Supplementary Fig. 7). This onset of metallic transport identifies  $T_{\rm BR}^{-19}$ ; while thermal fluctuations prevail at higher T, the quasiparticle bandwidth is the dominant energy scale for T <  $T_{\rm BR}$ . Below  $T_{\rm FL}$  the resistivity  $\rho(T) \propto T^2$  indicates the Fermi-liquid state (see Fig. 1).

Right at the first-order IMT, however, the dielectric behavior appears rather surprising. When approaching the low-temperature phase boundary,  $\varepsilon_1$  rapidly increases by several orders of magnitude. This colossal permittivity enhancement is more pronounced in the quasi-static limit,  $\varepsilon_1 \approx 10^5$  at f=7.5 kHz, and the peak value approximately follows a  $f^{-1.5}$  dependence. The overall range in T and p/x of the divergency is robust and does not depend on the probing frequency (see Supplementary Figs. 4 and 8).

In Fig. 3a, b the pressure evolution of  $\sigma_1$  and  $\varepsilon_1$  is plotted for fixed T. At T=10 K,  $\sigma_1(p)$  rises by six orders of magnitude in the narrow range of 1 kbar. This behavior flattens to a gradual transition above 20 K, associated with the quantum-critical crossover at the QWL. The inflection point shifts to higher p, in accord with the positive slope of the phase boundary  $^{15}$  associated with the rising onset of metallicity at  $T_{\rm BR}$ . The  $\kappa$ -STF $_{\rm x}$  series exhibits similar behavior (Fig. 3c, d): around the critical concentration of  $x\approx 0.12$  a drastic increase in  $\sigma_1$  is observed at low T that smears out as T rises. The maximum in  $\varepsilon_1(x)$  is reached for x=0.16 but broadens rapidly upon heating.

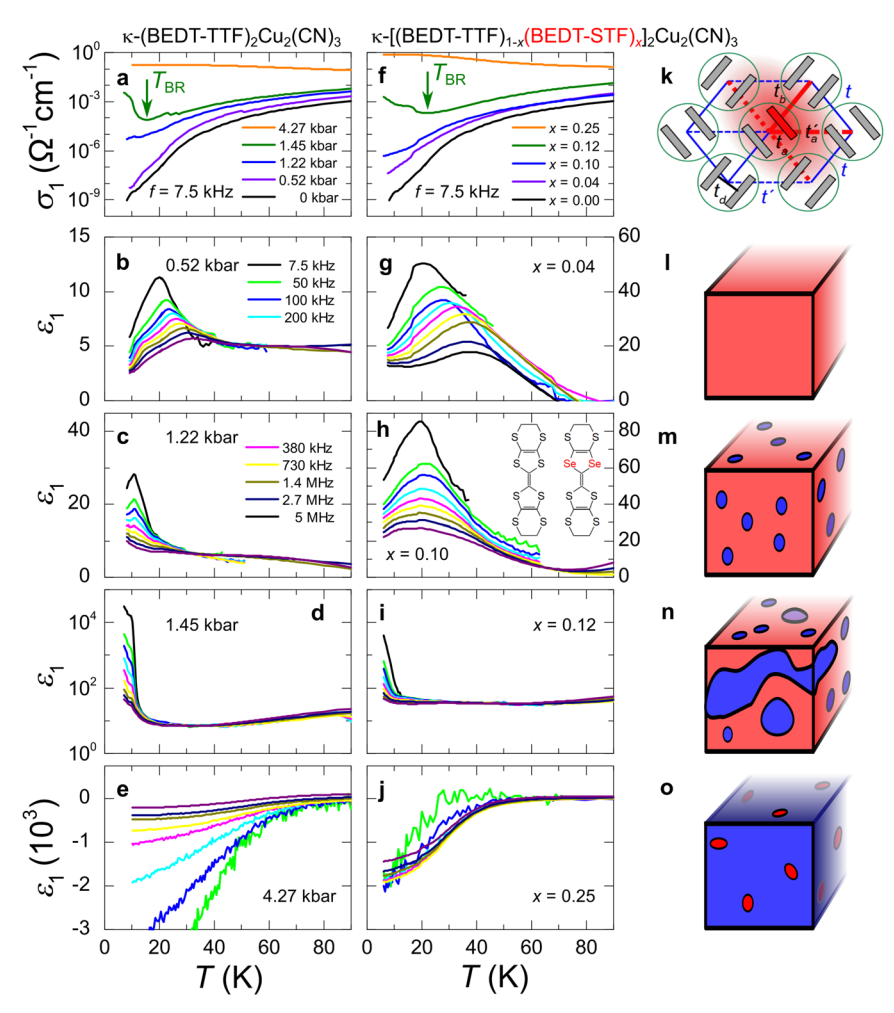


Fig. 2 Dielectric properties upon tuning through the Mott transition. The dielectric conductivity and permittivity of  $\kappa$ -(BEDT-TTF)<sub>2</sub>Cu<sub>2</sub>(CN)<sub>3</sub> were measured as a function of temperature and frequency for various applied **a**–**e** pressures and **f**–**j** chemical substitutions (introduction of Se-containing BEDT-STF molecules illustrated in **h** and **k**) that drive the system across the Mott transition. **a**, **f** Starting from the insulator,  $\sigma_1(T)$  grows with increasing p or x; a metallic phase is stabilized below  $T_{BR}$ , in accord with dc transport<sup>5,14,21</sup>. **b**, **c**, **g**, **h** In the Mott-insulating state  $\varepsilon_1(T)$  exhibits relaxor-ferroelectric behavior similar to the parent compound<sup>33,34</sup>. Extrinsic high-temperature contributions are subtracted. **d**, **i** The strong enhancement of  $\varepsilon_1(T)$  at the transition is a hallmark of a percolative IMT, as sketched in **I**–**o**. **e**, **j** When screening becomes dominant in the metal,  $\varepsilon_1$  turns negative;  $\sigma_1$  exhibits Fermi-liquid behavior below  $T_{FL}$ .

#### Modeling phase coexistence by hybrid DMFT

The Mott IMT is based on the physical picture that a reduction of electronic correlations (i.e., the rise of W/U) gradually closes the Mott-Hubbard gap: a coherent charge response develops, causing a finite metallic conductivity. Pressure-dependent optical studies on several organic Mott insulators indeed observe this behavior<sup>13,35</sup>. Concerning dielectric response, it was pointed out<sup>36</sup> that even in the case of certain continuous IMTs, the reduction of the charge gap might induce an enhancement in  $\varepsilon_1$ , perhaps leading to a divergence at low T. Probing the optical response at THz frequencies is actually a convenient method to monitor the gap contribution to the permittivity. From p and T sweeps across the Mott IMT of several different materials, an increase by a factor of 10 is consistently reported <sup>13,26</sup>; in the case of  $\kappa$ -STF<sub>x</sub> we find it to be even smaller (see Supplementary Fig. 7). Hence, the dielectric catastrophe of  $\varepsilon_1 \approx 10^5$  observed in our pressure and substitutiondependent dielectric experiments clearly signals a different mechanism at play.

To understand the physical origin of this anomaly, we recall the phase diagram of the Mott IMT at half filling, as obtained from DMFT<sup>6,7,37,38</sup>, which has been found to successfully describe many experimental features of QSL materials<sup>4,15</sup> such as ours. It features a first-order IMT at low temperatures ( $k_B T_{crit} \approx 0.02 W$ ), and an

associated phase-coexistence region over an appreciable range of U/W. As in most other systems displaying phase coexistence, here we expect spatial phase segregation of the respective metallic and insulating domains, with a relative volume fraction that smoothly varies with U/W. Such a picture resembles composite materials, such as microemulsions, composites or percolating metal films<sup>39–43</sup>. Here we expect percolation—a phenomenon that has been long studied in a number of spatially inhomogeneous systems—to distinctly affect all physical quantities. One of the prominent consequences is a strong enhancement of  $\varepsilon_1$  around the percolation transition, in addition to dramatic changes in the dc resistivity<sup>44–47</sup>.

While percolation theory is by now well understood, its specific experimental manifestation may be very sensitive to the physical properties of the coexisting phases, especially in strongly correlated systems. To theoretically investigate the physical consequences of such percolative effects for our Mott system, we set up a "Hybrid DMFT" simulation across the entire phase diagram. Here we utilized DMFT to calculate  $\varepsilon_1 + i\varepsilon_2$  for a singleband Hubbard model at half filling, and obtained the respective responses for both the insulating and the metallic phase as a function of T/W, U/W and frequency  $\omega/W$ . Using this information on the homogeneous phases as input to percolation theory, we



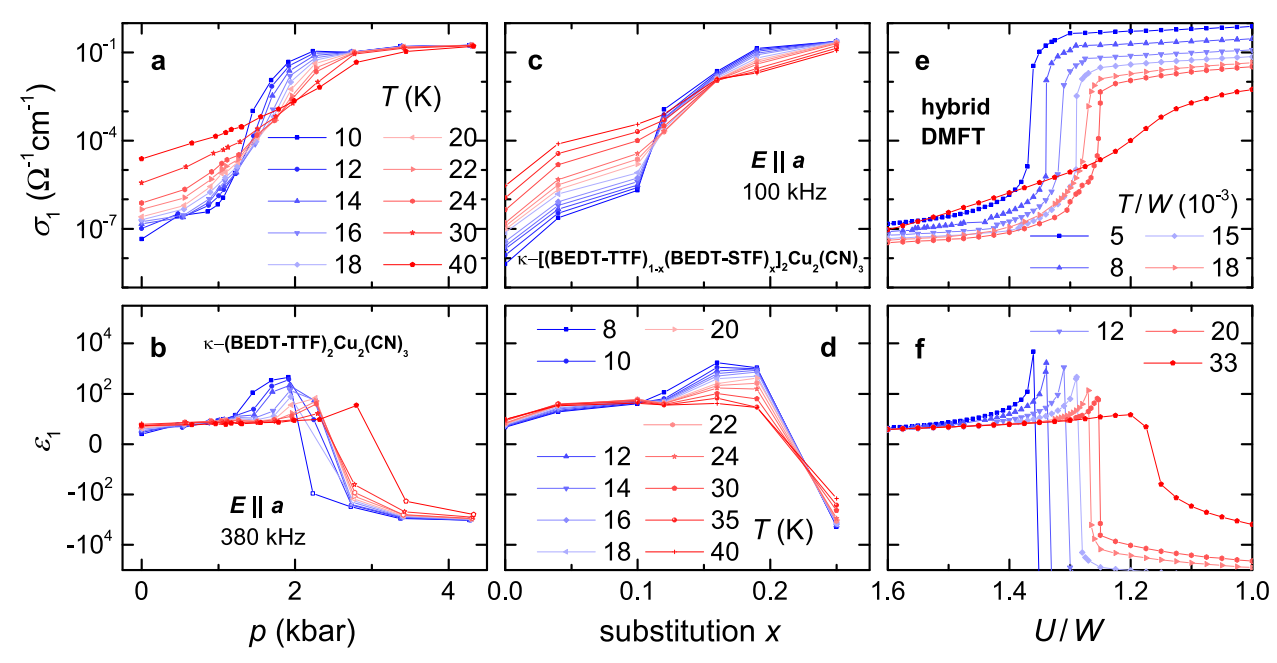


Fig. 3 Electrodynamics at the percolative Mott transition. a The Mott IMT of κ-(BEDT-TTF)<sub>2</sub>Cu<sub>2</sub>(CN)<sub>3</sub> appears as a rapid increase of  $\sigma_1(p)$  that smoothens at higher T; above  $T_{crit}$  a gradual crossover remains. b  $\varepsilon_1(p)$  exhibits a sharp peak below  $T_{crit}$ . The results at f=380 kHz are plotted on a logarithmic scale. c, d Similar behavior is observed for chemical BEDT-STF substitution x. e, f Fixed-temperature line cuts of our hybrid DMFT simulations (see text) as a function of correlation strength U/W and  $T/W^{15,16}$  resemble the experimental situation in minute detail, including the shift of the IMT with T. The lack of saturation of  $\sigma_1(T \to 0)$  seen in DMFT modeling reflects the neglect of elastic (impurity) scattering in the metal (outside the coexistence region).

then set up an appropriate random resistor network describing the dielectric properties within the phase-coexistence region, and solved it using standard effective-medium methods<sup>48</sup>, which suffices for our purposes.

We stress here that our Hybrid DMFT method provides a fully microscopic modeling for the physical properties of the respective phases across the phase diagram, a task that required a large-scale computational effort which we carried out in detail. In contrast, here we do not address the microscopic mechanism leading to the assumed phase separation, but instead adopt a phenomenological model (see Methods) describing how the relative volume fractions of the percolating species vary with T and U/W. In principle, spatial phase separation we envision may originate either from disorder effects<sup>49,50</sup>, or due to inherent ("Coulomb limited") phase separation<sup>51–53</sup>. In either case, one expects the relative volume fraction of the respective metallic/insulating components to smoothly vary with pressure, doping or temperature, and the resulting percolative effects should be very similar. We do not expect any of the resulting anomalies to depend on the details of our phenomenological model, e.g., the strong enhancement of the dielectric permittivity or the abrupt drop of the resistivity around the percolation point (see Supplementary Note 4 for a more detailed discussion of percolation phenomena in general).

Our hybrid DMFT simulation yields excellent agreement with experiment—both pressure tuning and chemical substitution—as illustrated in Fig. 3e, f and in the false-color plots in Fig. 4. We find that the colossal peak in  $\varepsilon_1$  is confined to the spatially inhomogeneous coexistence regime, exactly as observed in experiments. As correlation effects diminish, the dynamical conductivity (upper panels) increases from the Mott insulator to the Fermi liquid. The step in  $\sigma_1$  and drop in  $\varepsilon_1$  appear abruptly in the model but more smoothly in experiment, most likely due to inhomogeneities which broaden the coexistence regime in real materials by providing nucleation seeds for the incipient phase. Note, the percolative transition region narrows for  $T \rightarrow T_{crit}$  and vanishes above that; the metallic fraction m of the simulation is

indicated in Fig. 4f. The inset of panel f clearly demonstrates that the colossal permittivity enhancement appears exclusively for a percolating mixture of metallic and insulating regions, and not for the pure phases. These results render the gap closing irrelevant for the electrodynamics at the low-temperature Mott IMT. We further point out that the discussed mechanism of a percolative enhancement of  $\varepsilon_1$  may also apply to other related organic compounds, where similar dielectric anomalies at or nearby a first-order IMT were previously assigned to ferroelectricity<sup>54</sup> and multiferroicity<sup>55</sup>.

#### DISCUSSION

While previous transport and optical studies<sup>5,15</sup> already provided hints favoring the DMFT scenario, they do not map-out the predicted dynamical regimes, especially regarding a well-defined coexistence region at  $T < T_{crit}$ . Our pressure- and substitutiondependent dielectric data, however, reveal all phases in vivid detail and in remarkable agreement with the respective crossover lines obtained from dc transport. Indeed, we recognize the gapped Mott insulator by essentially constant  $\varepsilon_1$  (light red) bounded precisely by the QWL<sup>16</sup>, while also below  $T_{\rm BR}^{19,20}$  the response clearly follows the dielectric behavior expected for a metal ( $\varepsilon_1$  < 0, blue). Most remarkably, these two crossover lines converge towards  $T_{crit}$  which marks the onset of the coexistence region, just as anticipated from Fig. 1. The emergence of phase segregation is evidenced by the huge peak of  $\varepsilon_1$  in excellent agreement with our current DMFT-based modeling. The sharply defined boundaries of this dielectric anomaly imply that the corresponding inhomogeneities are the consequence and not the cause of phase separation, the latter resulting from strong correlation effects inherent to Mottness. Our findings substantiate that the DMFT scenario offers a rather accurate picture of the Mott IMT, in contrast to other theoretical viewpoints<sup>56</sup>, which focus on the spin degrees of freedom in the QSL. This also confirms recent experimental and theoretical results<sup>57,58</sup> suggesting that such gapless spin excitations, while dominant deep within the

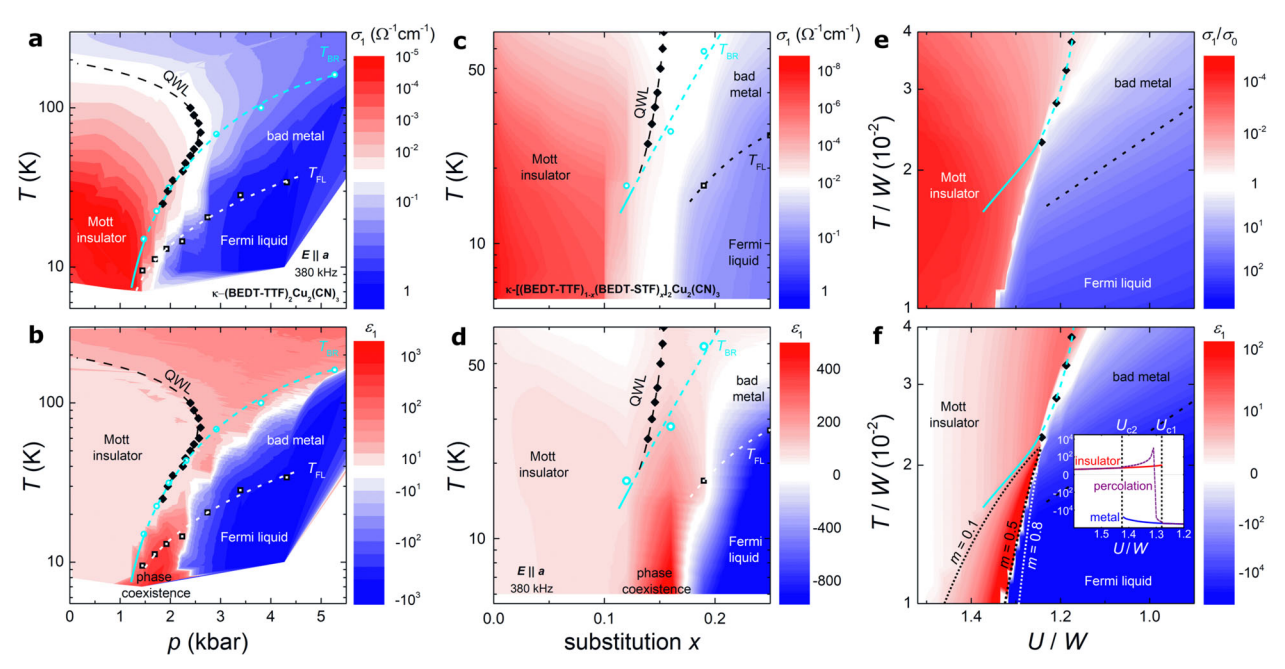


Fig. 4 Phase diagram of  $\kappa$ -(BEDT-TTF)<sub>2</sub>Cu<sub>2</sub>(CN)<sub>3</sub> when tuned through the Mott IMT. Both conductivity and permittivity exhibit similar behavior upon varying correlation strength U/W by **a**, **b** physical pressure or **c**, **d** chemical substitution, which is reproduced by **e**, **f** our hybrid DMFT calculations; the respective color codes are given to the right. In all cases, the colossal enhancement of  $\varepsilon_1$  reveals a sharply defined insulator-metal phase-coexistence region around the first-order IMT, which is not seen in  $\sigma_1$ . The permittivity clearly distinguishes the Mott-insulating and metallic states via small positive and large negative values, which line up perfectly with the quantum Widom line (QWL) and the Brinkman-Rice temperature  $T_{BR}$  determined from  $\sigma_1(T, p, x)$ , respectively. Inset of **f**: metallic and insulating DMFT solutions are contrasted to the mixed phase (metallic fractions m indicated in main panel) that reproduces the strong peak in  $\varepsilon_1$ . Note,  $T_{BR}$  is indicated by a dashed cyan line at  $T > T_{crit}$  in all panels; the resistivity maxima below  $T_{crit}$  (solid cyan line) arise due to percolative effects.

low-temperature Mott-insulating phase, are quickly damped away by the onset of charge fluctuations close to the IMT.

We demonstrated an expedient method of partial chemical substitution that triggers a similar Mott transition in  $\kappa$ -(BEDT-TTF)<sub>2</sub>Cu<sub>2</sub>(CN)<sub>3</sub> as physical pressure. The pronounced divergency in  $\epsilon_1$ , occuring for both types of bandwidth tuning, evidences a spatial coexistence of metallic and insulating electronic phases around the first-order IMT that can be circumstantially described by DMFT blended with percolation theory. Our results yield that the Mott gap has a minor effect on the dielectric properties while the effects of phase coexistence dominate.

#### **METHODS**

#### **Experimental**

High-quality single crystals of κ-(BEDT-TTF)<sub>2</sub>Cu<sub>2</sub>(CN)<sub>3</sub> were grown by the standard electrochemical synthesis method 59,60 at Stuttgart and at Argonne. Plate-like single crystals of  $\kappa$ -[(BEDT-TTF)<sub>1-x</sub>(BEDT-STF)<sub>x</sub>]<sub>2</sub>Cu<sub>2</sub>(CN)<sub>3</sub> with a typical size of  $1 \times 1 \times 0.3$  mm<sup>3</sup> were prepared according to ref. <sup>61</sup> here BEDT-TTF stands for bis(ethylenedithio)tetrathiafulvalene. Substituting two of the inner sulfur atoms by selenium leads to bis-ethylenedithiodiselenium-dithiafulvalene, abbreviated BEDT-STF. Energy-dispersive X-ray spectroscopy was employed to determine the chemical composition of the alloys  $0 \le x \le 1^{61}$ . The complex impedance of the crystals was measured as a function of temperature and frequency to obtain the permittivity  $\hat{\epsilon}=$  $\epsilon_1+i\epsilon_2$  and the conductivity  $\hat{\sigma}=\sigma_1+i\sigma_2$ . The crystals are contacted outof-plane (E||a) by attaching thin gold wires with carbon paint to the opposite crystal surfaces. The measurements were performed with two contacts in a pseudo four-point configuration using an Agilent 4294 Impedance Analyzer. The applied ac voltage was set to 0.5 V, which was still in the Ohmic regime.

For the pressure-dependent experiments on the  $\kappa$ -(BEDT-TTF)<sub>2</sub>Cu<sub>2</sub>(CN)<sub>3</sub> crystals, we used a piston-type pressure cell ranging up to 10 kbar with a self-made electrical feedthrough for coaxial cables designed for pressure-dependent dielectric spectroscopy measurements as described in detail elsewhere<sup>62</sup>. Daphne oil 7373 was used as liquid pressure-transmitting medium because it is inert to molecular solids, has a good hydrostaticity

and stays fluid at room temperature for all applied pressures. The inherent pressure loss upon cooling was recorded continuously in situ by an InSb semiconductor pressure gauge<sup>63</sup>, which shows a negligible pressure gradient below 50 K. The main temperature range discussed here is collected from the same pressure cycles; and the pressure reading at 10 K is given throughout the manuscript, unless stated otherwise. A continuous flow cryostat was utilized to cool down the pressure cell. A total cable length of only 50 cm enables measurements up to 5 MHz. The rather steep thermal gradient limits the lowest reachable temperature to 8 K, hence the superconducting state at  $T \approx 4 \text{ K}^{14,21}$  was not accessible to our dielectric experiments. No dependence on the cooling rate was observed, which was kept below 0.4 K/min for all measurements. Additional data, including analysis on the frequency dependence, can be found in Supplementary Notes 2 and 3.

#### Dynamical mean-field theory modeling

We performed standard<sup>6,20</sup> DMFT calculations of the optical conductivity  $\sigma_1$  of a single-band Hubbard model at 1/2-filling, using a semicircular model density of states and iterated perturbation theory as an impurity solver, which suffices 16,17 for our purposes. The imaginary part of conductivity  $\sigma_2$  was then obtained via the Kramers–Kronig transformation, and the dielectric function  $\epsilon(\omega)=1+irac{4\pi}{\omega}\sigma(\omega)$  was obtained across the entire phase diagram, for both uniform phases. To describe percolative effects within the phase-coexistence region, we assumed spatial segregation of metallic and insulating regions with a smoothly varying metallic filling fraction. We used the standard effective-medium theory<sup>64</sup> corresponding random conductor/dielectric network, with a binary distribution of the local dielectric functions as calculated from DMFT for given temperature T and Coulomb repulsion U. All energies are expressed in units of the bandwidth W, i.e., T/W and U/W. For simplicity, we assign a smooth hyperbolic tangent function, as routinely used to describe phase coexistence near any first-order phase transition<sup>49</sup>, to model the volume fraction of the metallic phase:  $m(T/W, U/W) = \frac{1}{2} \tanh \{c[(T/W)_{crit} - T/W]/$  $[(U/W)_{crit} - U/W]\} + \frac{1}{2}$ , which is centered around the middle of the coexistence region:  $(U/W)_{crit} = (0.20 - T/W)/0.14$ . In order to match the coexistence region with the experimental data, we selected c = 0.1 for U/W> (U/W)<sub>crit</sub> and c=0.3 for U/W < (U/W)<sub>crit</sub>. More details and a visualization of the assumed metallic fraction m can be found in Supplementary Note 4.



#### **DATA AVAILABILITY**

The authors declare that the data supporting the findings of this study are available within the paper and its Supplementary information. For further details, contact A.P., V.D., or M.D.

Received: 3 July 2020; Accepted: 11 December 2020;

#### Published online: 27 January 2021

#### REFERENCES

- Shklovskii, B. I. & Efros, A. L. Electronic properties of doped semiconductors (Springer-Verlag, Berlin, 1984).
- Imada, M., Fujimori, A. & Tokura, Y. Metal-insulator transitions. Rev. Mod. Phys. 70, 1039–1263 (1998).
- Kanoda, K. & Kato, R. Mott physics in organic conductors with triangular lattices. Annu. Rev. Condens. Matter Phys. 2, 167–188 (2011).
- Powell, B. J. & McKenzie, R. H. Quantum frustration in organic Mott insulators: from spin liquids to unconventional superconductors. *Rep. Prog. Phys.* 74, 56501 (2011).
- Furukawa, T., Miyagawa, K., Taniguchi, H., Kato, R. & Kanoda, K. Quantum criticality of Mott transition in organic materials. *Nat. Phys.* 11, 221–224 (2015).
- Georges, A., Kotliar, G., Krauth, W. & Rozenberg, M. J. Dynamical mean-field theory of strongly correlated fermion systems and the limit of infinite dimensions. *Rev. Mod. Phys.* 68, 13–125 (1996).
- Vollhardt, D. Dynamical mean-field theory for correlated electrons. Ann. Phys. (Berl.) 524, 1–19 (2012).
- Limelette, P. et al. Universality and critical behavior at the Mott transition. Science 302, 89 – 92 (2003).
- Limelette, P. et al. Mott transition and transport crossovers in the organic compound κ-(BEDT-TTF)<sub>2</sub>Cu[N(CN)<sub>2</sub>]Cl. Phys. Rev. Lett. 91, 016401 (2003).
- Hansmann, P. et al. Mott-Hubbard transition in V<sub>2</sub>O<sub>3</sub> revisited. *Phys. Status Solidi B* 250, 1251–1264 (2013).
- Shimizu, Y. et al. Pressure-tuned exchange coupling of a quantum spin liquid in the molecular triangular lattice κ-(BEDT-TTF)<sub>2</sub>Ag<sub>2</sub>(CN)<sub>3</sub>. Phys. Rev. Lett. 117, 107203 (2016).
- Itou, T. et al. Slow dynamics of electrons at a metal-Mott insulator boundary in an organic system with disorder. Sci. Adv. 3, e1601594 (2017).
- Li, W., Pustogow, A., Kato, R. & Dressel, M. Transition of a pristine Mott insulator to a correlated Fermi liquid: Pressure-dependent optical investigations of a quantum spin liquid. Phys. Rev. B 99, 115137 (2019).
- Furukawa, T., Kobashi, K., Kurosaki, Y., Miyagawa, K. & Kanoda, K. Quasicontinuous transition from a Fermi liquid to a spin liquid in κ-(ET)<sub>2</sub>Cu<sub>2</sub>(CN)<sub>3</sub>. Nat. Commun. 9, 307 (2018).
- Pustogow, A. et al. Quantum spin liquids unveil the genuine Mott state. Nat. Mater. 17, 773–777 (2018).
- Vučičević, J., Terletska, H., Tanasković, D. & Dobrosavljević, V. Finite-temperature crossover and the quantum Widom line near the Mott transition. *Phys. Rev. B* 88, 075143 (2013).
- Terletska, H., Vučičević, J., Tanasković, D. & Dobrosavljević, V. Quantum critical transport near the Mott transition. *Phys. Rev. Lett.* 107, 026401 (2011).
- Dobrosavljević, V., Abrahams, E., Miranda, E. & Chakravarty, S. Scaling theory of two-dimensional metal-insulator transitions. Phys. Rev. Lett. 79, 455–458 (1997).
- Radonjić, M. M., Tanasković, D., Dobrosavljević, V., Haule, K. & Kotliar, G. Wigner-Mott scaling of transport near the two-dimensional metal-insulator transition. *Phys. Rev. B* 85, 085133 (2012).
- Deng, X. et al. How bad metals turn good: Spectroscopic signatures of resilient quasiparticles. Phys. Rev. Lett. 110, 086401 (2013).
- Kurosaki, Y., Shimizu, Y., Miyagawa, K., Kanoda, K. & Saito, G. Mott transition from a spin liquid to a Fermi liquid in the spin-frustrated organic conductor κ-(BEDT-TTF)<sub>2</sub>Cu<sub>2</sub>(CN)<sub>3</sub>. *Phys. Rev. Lett.* **95**, 177001 (2005).
- Zaanen, J., Sawatzky, G. A. & Allen, J. W. Band gaps and electronic structure of transition-metal compounds. *Phys. Rev. Lett.* 55, 418–421 (1985).
- Acharya, S. et al. Metal-insulator transition in copper oxides induced by apex displacements. Phys. Rev. X 8, 021038 (2018).
- Lefebvre, S. et al. Mott transition, antiferromagnetism, and unconventional superconductivity in layered organic superconductors. *Phys. Rev. Lett.* 85, 5420–5423 (2000)
- Sasaki, T., Yoneyama, N., Kobayashi, N., Ikemoto, Y. & Kimura, H. Imaging phase separation near the Mott boundary of the correlated organic superconductors κ-(BEDT-TTF)<sub>2</sub>X. Phys. Rev. Lett. 92, 227001 (2004).
- Qazilbash, M. M. et al. Mott transition in VO<sub>2</sub> revealed by infrared spectroscopy and nano-imaging. Science 318, 1750–1753 (2007).

- Lupi, S. et al. A microscopic view on the Mott transition in chromium-doped V<sub>2</sub>O<sub>3</sub>.
   Nat. Commun. 1, 105 (2010).
- 28. McLeod, A. S. et al. Nanotextured phase coexistence in the correlated insulator  $V_2O_3$ . Nat. Phys. 13, 80–86 (2016).
- Post, K. W. et al. Coexisting first- and second-order electronic phase transitions in a correlated oxide. Nat. Phys. 14, 1056–1061 (2018).
- Pustogow, A., McLeod, A. S., Saito, Y., Basov, D. N. & Dressel, M. Internal strain tunes electronic correlations on the nanoscale. Sci. Adv. 4, eaau9123 (2018).
- Kézsmárki, I. et al. Depressed charge gap in the triangular-lattice Mott insulator κ-(BEDT-TTF)<sub>2</sub>Cu<sub>2</sub>(CN)<sub>3</sub>. Phys. Rev. B 74, 201101 (2006).
- Čulo, M. et al. Hall effect study of the κ-(BEDT-TTF)<sub>2</sub>X family: evidence for Mott-Anderson localization. *Phys. Rev. B* 99, 045114 (2019).
- Abdel-Jawad, M. et al. Anomalous dielectric response in the dimer Mott insulator κ-(BEDT-TTF)<sub>2</sub>Cu<sub>2</sub>(CN)<sub>3</sub>. Phys. Rev. B 82, 125119 (2010).
- Pinterić, M. et al. Anisotropic charge dynamics in the quantum spin-liquid candidate κ-(BEDT-TTF)<sub>2</sub>Cu<sub>2</sub>(CN)<sub>3</sub>. Phys. Rev. B 90, 195139 (2014).
- Faltermeier, D. et al. Bandwidth-controlled Mott transition in κ-(BEDT-TTF)<sub>2</sub>Cu[N (CN)<sub>2</sub>]Br<sub>x</sub>Cl<sub>1-x</sub>: optical studies of localized charge excitations. *Phys. Rev. B* 76, 165113 (2007).
- Aebischer, C., Baeriswyl, D. & Noack, R. M. Dielectric catastrophe at the Mott transition. *Phys. Rev. Lett.* 86, 468–471 (2001).
- Kotliar, G. & Vollhardt, D. Strongly correlated materials: Insights from dynamical mean-field theory. *Phys. Today* 57, 53–59 (2004).
- Vollhardt, D. Dynamical mean-field theory of strongly correlated electron systems. JPS Conf. Proc. 30, 011001 (2020).
- van Dijk, M. A., Casteleijn, G., Joosten, J. G. H. & Levine, Y. K. Percolation in oilcontinuous microemulsions. A dielectric study of aerosol OT/water/isooctane. J. Chem. Phys. 85, 626–631 (1986).
- Clarkson, M. T. & Smedley, S. I. Electrical conductivity and permittivity measurements near the percolation transition in a microemulsion: I. Experiment. *Phys. Rev.* A 37, 2070–2078 (1988).
- Pecharromán, C. & Moya, J. S. Experimental evidence of a giant capacitance in insulator-conductor composites at the percolation threshold. *Adv. Mater.* 12, 294–297 (2000).
- Nan, C.-W., Shen, Y. & Ma, J. Physical properties of composites near percolation. Ann. Rev. Mater. Res. 40, 131–151 (2010).
- Hövel, M., Gompf, B. & Dressel, M. Dielectric properties of ultrathin metal films around the percolation threshold. *Phys. Rev. B* 81, 035402 (2010).
- Dubrov, V. E., Levinshtein, M. E. & Shur, M. S. Permittivity anomaly in metaldielectric transitions. Theory and simulation. *J. Exp. Theor. Phys.* 43, 1050–1056 (1976)
- Efros, A. L. & Shklovskii, B. I. Critical behaviour of conductivity and dielectric constant near the metal-non-metal transition threshold. *Phys. Status Solidi B* 76, 475–485 (1976).
- Bergman, D. J. & Imry, Y. Critical behavior of the complex dielectric constant near the percolation threshold of a heterogeneous material. *Phys. Rev. Lett.* 39, 1222–1225 (1977).
- Bergman, D. J. The dielectric constant of a composite material A problem in classical physics. *Phys. Rep.* 43, 377–407 (1978).
- 48. Choy, T. C. Effective medium theory: Principles and applications, 2nd edn (Oxford University Press, Oxford, 2015).
- Dagotto, E. Nanoscale phase separation and colossal magnetoresistance: The physics of manganites and related compounds (Springer-Verlag, New York, 2002)
- Suárez-Villagrán, M. Y. et al. Two-dimensional disordered Mott metal-insulator transition. Phys. Rev. B 101, 235112 (2020).
- Schmalian, J. & Wolynes, P. G. Stripe glasses: self-generated randomness in a uniformly frustrated system. *Phys. Rev. Lett.* 85, 836–839 (2000).
- Eckstein, M., Kollar, M., Potthoff, M. & Vollhardt, D. Phase separation in the particle-hole asymmetric Hubbard model. *Phys. Rev. B* 75, 125103 (2007).
- Terletska, H. & Dobrosavljević, V. Fingerprints of intrinsic phase separation: magnetically doped two-dimensional electron gas. *Phys. Rev. Lett.* 106, 186402 (2011).
- Gati, E. et al. Evidence for electronically driven ferroelectricity in a strongly correlated dimerized BEDT-TTF molecular conductor. *Phys. Rev. Lett.* 120, 247601 (2018).
- Lunkenheimer, P. et al. Multiferroicity in an organic charge-transfer salt that is suggestive of electric-dipole-driven magnetism. Nat. Mater. 11, 755–758 (2012).
- Senthil, T. Theory of a continuous Mott transition in two dimensions. *Phys. Rev. B* 78, 045109 (2008).
- Lee, T.-H., Florens, S. & Dobrosavljević, V. Fate of spinons at the Mott point. Phys. Rev. Lett. 117, 136601 (2016).
- Pustogow, A. et al. Low-energy excitations in quantum spin liquids identified by optical spectroscopy. Phys. Rev. Lett. 121, 056402 (2018).

np.

- Geiser, U. et al. Superconductivity at 2.8 K and 1.5 kbar in κ-(BEDT-TTF)<sub>2</sub>Cu<sub>2</sub>(CN)<sub>3</sub>: the first organic superconductor containing a polymeric copper cyanide anion. *Inorg. Chem.* 30, 2586–2588 (1991).
- Komatsu, T., Matsukawa, N., Inoue, T. & Saito, G. Realization of superconductivity at ambient pressure by band-filling control in κ-(BEDT-TTF)<sub>2</sub>Cu<sub>2</sub>(CN)<sub>3</sub>. J. Phys. Soc. Jpn. 65, 1340–1354 (1996).
- Saito, Y., Minamidate, T., Kawamoto, A., Matsunaga, N. & Nomura, K. Site-specific
   <sup>13</sup>C NMR study on the locally distorted triangular lattice of the organic conductor
   κ-(BEDT-TTF)<sub>2</sub>Cu<sub>2</sub>(CN)<sub>3</sub>. Phys. Rev. B 98, 205141 (2018).
- 62. Rösslhuber, R., Uykur, E. & Dressel, M. Pressure cell for radio-frequency dielectric measurements at low temperatures. *Rev. Sci. Instrum.* **89**, 054708 (2018).
- Beyer, R. & Dressel, M. Piston pressure cell for low-temperature infrared investigations. Rev. Sci. Instrum. 86, 053904 (2015).
- 64. Kirkpatrick, S. Percolation and conduction. Rev. Mod. Phys. 45, 574-588 (1973).

#### **ACKNOWLEDGEMENTS**

We thank G. Untereiner for contacting the crystals and S. Brown for fruitful discussions. We acknowledge funding by the DFG via DR228/52-1 and DR228/39-3. A. P. acknowledges support by the Alexander von Humboldt Foundation through the Feodor Lynen Fellowship. Work in Florida was supported by the NSF Grant No. 1822258, and the National High Magnetic Field Laboratory through the NSF Cooperative Agreement No. 1157490 and the State of Florida. E.U. receives support of the European Social Fund and the Ministry of Science Research and the Arts of Baden-Württemberg. J.A.S. acknowledges support from the Independent Research/ Development program while serving at the National Science Foundation.

#### **AUTHOR CONTRIBUTIONS**

Dielectric spectroscopic investigations were conceived by M.D. R.R. designed and performed the experiments, supported by E.U., A.B., M.W., and Y.S. Y.T. and V.D. carried out theoretical calculations. A.P. initiated and steered the collaboration of experiment and theory. A.L., R.H., Y.S., A.K., and J.A.S. prepared the crystals. A.P., M.D., and V.D. discussed the data, interpreted the results, and wrote the paper with input from all authors. A.P., R.R., and Y.T. contributed equally to this work.

#### **FUNDING**

Open Access funding enabled and organized by Projekt DEAL.

#### **COMPETING INTERESTS**

The authors declare no competing interests.

#### ADDITIONAL INFORMATION

**Supplementary information** is available for this paper at https://doi.org/10.1038/s41535-020-00307-0.

Correspondence and requests for materials should be addressed to A.P., V.D. or M.D.

Reprints and permission information is available at http://www.nature.com/reprints

**Publisher's note** Springer Nature remains neutral with regard to jurisdictional claims in published maps and institutional affiliations.

Open Access This article is licensed under a Creative Commons Attribution 4.0 International License, which permits use, sharing, adaptation, distribution and reproduction in any medium or format, as long as you give appropriate credit to the original author(s) and the source, provide a link to the Creative Commons license, and indicate if changes were made. The images or other third party material in this article are included in the article's Creative Commons license, unless indicated otherwise in a credit line to the material. If material is not included in the article's Creative Commons license and your intended use is not permitted by statutory regulation or exceeds the permitted use, you will need to obtain permission directly from the copyright holder. To view a copy of this license, visit http://creativecommons.org/licenses/by/4.0/.

© The Author(s) 2021

#### Supplementary Information

# Low-Temperature Dielectric Anomaly Arising from Electronic Phase Separation at the Mott Insulator-Metal Transition

A. Pustogow\*, 1,2 R. Rösslhuber\*, 1 Y. Tan\*, 3 E. Uykur, 1 A. Böhme, 1 M. Wenzel, 1 Y. Saito, 1,4 A. Löhle, 1 R. Hübner, 1,5 A. Kawamoto, 4 J. A. Schlueter, 6,7 V. Dobrosavljević, 3 and M. Dressel 1 1. Physikalisches Institut, Universität Stuttgart, 70569 Stuttgart, Germany 2 Department of Physics and Astronomy, UCLA, Los Angeles, California 90095, U.S.A. 3 National High Magnetic Field Laboratory, Florida State University, Tallahassee, U.S.A. 4 Department of Physics, Hokkaido University, Sapporo, Japan 5 Institut für Klinische Radiologie und Nuklearmedizin, Universität Heidelberg, Mannheim, Germany 6 Material Science Division, Argonne National Laboratory, Argonne, Illinois 60439-4831, U.S.A. 7 Division of Materials Research, National Science Foundation, Alexandria, Virginia 22314, U.S.A.

#### CONTENTS

Supplementary Note 1: Characterization of  $\kappa$ -(BEDT-TTF)<sub>2</sub>Cu<sub>2</sub>(CN)<sub>3</sub> by pressure and chemical substitution 1

Supplementary Note 2: Dielectric response as a function of pressure 3

Supplementary Note 3: Dielectric Response as a function of chemical substitution 6

Supplementary Note 4: Theoretical analysis of the dielectric permittivity at the IMT 8

Supplementary References 10

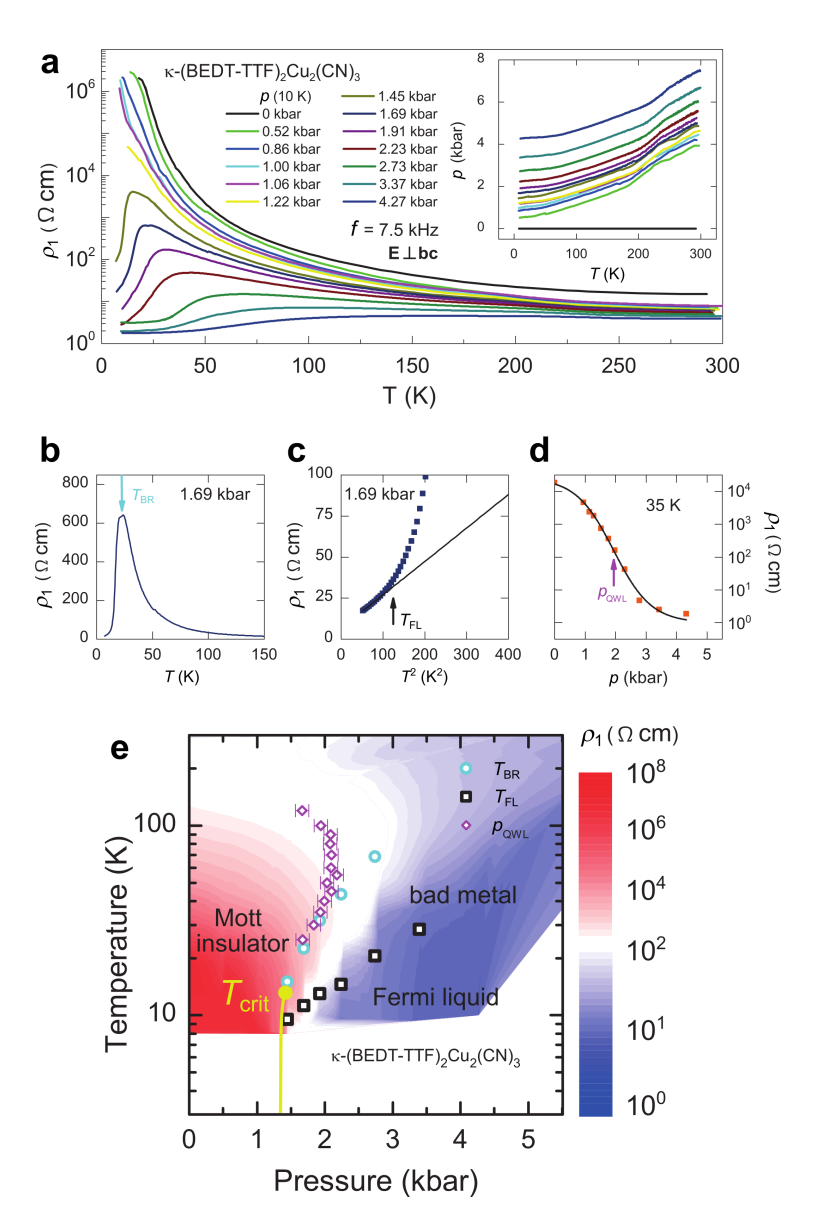
## SUPPLEMENTARY NOTE 1: CHARACTERIZATION OF $\kappa$ -(BEDT-TTF) $_2$ Cu $_2$ (CN) $_3$ BY PRESSURE AND CHEMICAL SUBSTITUTION

High-quality single crystals of  $\kappa$ -(BEDT-TTF)<sub>2</sub>Cu<sub>2</sub>(CN)<sub>3</sub> were grown by the standard electrochemical synthesis method [1, 2] at the Universität Stuttgart and Argonne National Laboratory. We measured the complex electrical impedance as a function of pressure, temperature and frequency in order to obtain the permittivity  $\hat{\varepsilon} = \varepsilon_1 + i\varepsilon_2$  or, equivalently, complex conductivity  $\hat{\sigma} = \sigma_1 + i\sigma_2$ . To that end, the crystals are contacted by attaching thin gold wires with carbon paint to opposite crystal surfaces, such that the measurements were performed out-of-plane with  $E \perp bc$ . The experiments were performed with two contacts in a pseudo four-point configuration [3] using an Agilent 4294 impedance analyzer. The applied ac voltage was set to 0.5 V, making sure that we operate in the Ohmic regime. In order to characterize the crystals, we have measured the low-frequency resistivity as a function of temperature and pressure, shown in Supplementary Figure 1.

For pressure-dependent dielectric experiments we utilized a piston-type pressure cell ranging up to approximately 10 kbar with a self-made electrical feedthrough for coaxial cables, which is described in detail in Supplementary Reference 6. Daphne oil 7373 was used as liquid pressure-transmitting medium because it is inert to molecular solids, has a good hydrostaticity, and stays fluid at room temperature for all applied pressures. The inherent pressure loss upon cooling was recorded *in-situ* by an InSb semiconductor pressure gauge that shows a negligible pressure gradient below T=50 K. As a consequence, in the temperature range of particular interest here, the data are collected in the same pressure cycles; this is important for comparison. Unless indicated otherwise, throughout the manuscript we state the pressure reading at T=10 K.

The pressure cell was cooled down in a custom-made continuous-flow helium cryostat that allows us to reduce the total cable length to 50 cm enabling reliable measurements at frequencies up to 5 MHz. The compact cryostat design results in a rather steep thermal gradient limiting the lowest reachable temperature to about 8 K. No dependence on the cooling rate was observed, which was kept below 0.4 K/min for all measurements. Performing similar experiments on different single crystals yields good agreement with the results presented here.

Supplementary Figure 1 displays the out-of-plane resistivity  $\rho_1(T)$  curves probed at low frequency. The indicated pressure values were recorded at T=10 K. Although these are two-point measurements, the results are in good

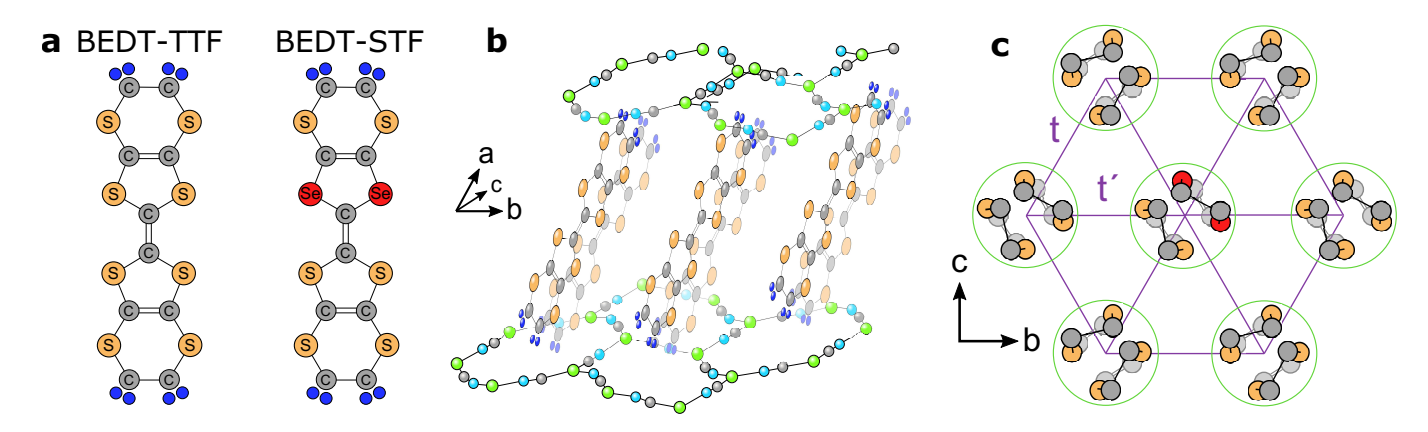


Supplementary Figure 1. **a**, Temperature-dependent out-of-plane resistivity  $\rho_1(T)$  of  $\kappa$ -(BEDT-TTF)<sub>2</sub>Cu<sub>2</sub>(CN)<sub>3</sub> for sample 2 under hydrostatic pressure, measured along the a-direction and at f=7.5 kHz, which is in good agreement with dc-measurements known from literature [4, 5]. With increasing pressure,  $\rho_1(T)$  is reduced, revealing the insulator-metal transition for p>1.45 kbar. The inset in panel **a** displays the *in-situ* measured pressure loss upon cooling. **b**, The maximum in  $\rho_1(T)$  (cyan arrow) directly indicates the onset of metallic conduction at the Brinkman-Rice temperature  $T_{\rm BR}$ . **c**, We define  $T_{\rm FL}$  as the temperature at which  $\rho_1$  deviates from  $\rho_{1,\rm FL}=\rho_0+AT^2$  by more then 10%. **d**, The quantum Widom line is determined by fitting  $\rho_1(p)$  (orange squares) at constant temperature with  $\log(\rho_{1,\rm QWL})=c[1-\tanh\{b(p-p_{\rm QWL})\}]$  (black line). **e**, Phase diagram which is based on a contour plot of  $\rho_1(p,T)$ , including  $T_{\rm max}$ ,  $T_{\rm FL}$  and  $p_{\rm QWL}$ . The yellow line represents an estimate of the Mott transition with a critical end point at  $T_{\rm crit}=1.45$  kbar.

agreement with the four-point dc-measurements reported in literature [4, 5], taking into account that we probe the perpendicular direction. For both samples we observe a maximum in  $\rho_1(T)$  that shifts to higher T with increasing pressure; concomitantly the resistivity is reduced.

The resistivity maximum at the Brinkman-Rice temperature  $T_{\rm BR}$  indicates the onset of the metallic transport regime with  ${\rm d}\rho_1/{\rm d}T < 0$ . The Fermi-liquid regime is characterized by  $\rho_1(T) = \rho_0 + AT^2$ . We define  $T_{\rm FL}$  as the temperature where  $\rho_1(T)$  deviates by more than 10% from this quadratic behavior. We remind here, that the experimental setup did not allow for cooling below 8 K such that the superconducting state below  $T_{\rm SC} = 4$  K could not be reached.

The inset in Supplementary Figure 1a shows the decrease of the *in-situ* recorded pressure upon cooling. The step like features around 220 K correspond to the solidification temperature of the pressure transmitting oil. Below 50 K,



Supplementary Figure 2. **a**, Organic donor molecules bis-(ethylenedithio)-tetrathiafulvalene, called BEDT-TTF, and bis-(ethylenedithio)-diseleniumdithiafulvalene, abbreviated BEDT-STF. In the latter case two sulfur atoms of the inner rings are replaced by selenium. **b**, The crystal structure contains dimers of the donor molecules forming layers in the bc-plane which are separated by the  $Cu_2(CN)_3$  anion sheets. **c**, The dimers are arranged in a triangular pattern with transfer integrals t'/t = 0.83 [10] close to complete frustration. The STF-substitution leads to a spatially random extension of the transfer integrals due to the larger molecular orbitals.

the pressure saturates and becomes nearly temperature-independent. For the 0 kbar measurement, the sample was cooled in the pressure cell, which was left open, only filled with He contact gas, such that pressure loss upon cooling is negligible.

The precise in-situ measurement of p(T) enables us to analyze  $\rho_1(p)$  at constant temperature. In particular, we determine the quantum Widom line (QWL) by fitting  $\rho_1(p)$  (orange squares) at constant temperature with  $\log\{\rho_1\} = c[1 - \tanh\{b(p - p_{\text{QWL}})\}]$  (black line), as examplarily shown in Supplementary Figure 1d. This procedure [7, 8] yields the QWL as the point of inflection at  $p_{\text{QWL}}$  which is indicated by the magenta arrow.

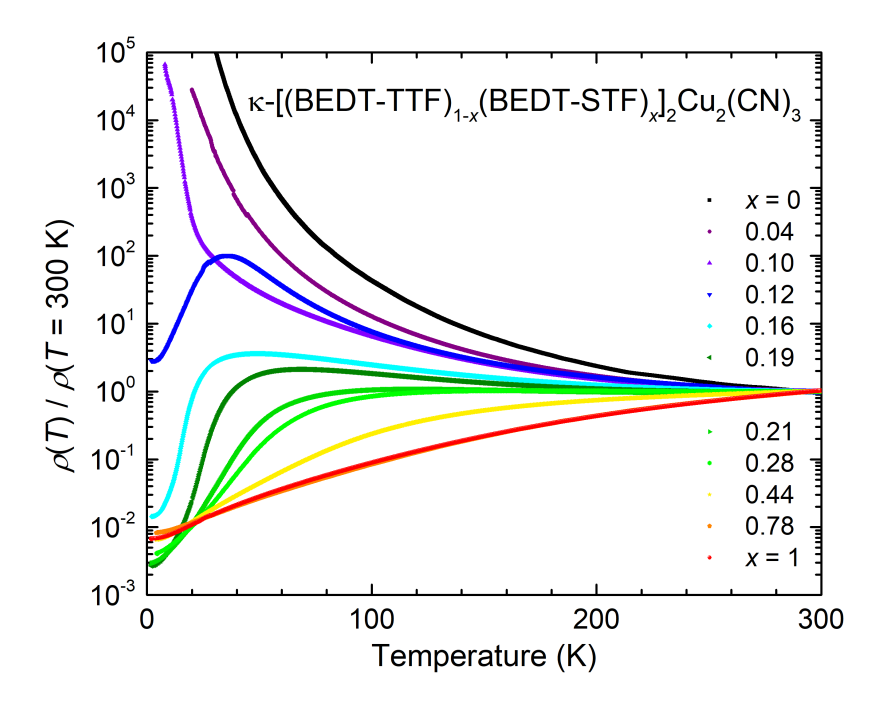
 $\kappa$ -[(BEDT-STF)<sub>x</sub>(BEDT-TTF)<sub>1-x</sub>]<sub>2</sub>Cu<sub>2</sub>(CN)<sub>3</sub> single crystals with varying stoichiometry (x=0, 0.04, 0.1, 0.12, 0.16, 0.19, 0.21, 0.25, 0.28, 0.44, 0.78 and 1) were prepared by standard electrochemical oxidation [1]. Both BEDT-TTF and BEDT-STF (molecules displayed in Supplementary Figure 2a) were synthesized at Hokkaido University in Sapporo, where also the crystal growth is carried out. For the alloying series, the amount of donor molecules was preselected; for each batch the actual substitution value <math>x was determined a posteriori by energy-dispersive x-ray spectroscopy: using  $\kappa$ -(BEDT-TTF)<sub>2</sub>Cu<sub>2</sub>(CN)<sub>3</sub> as a reference we compared the intensity of S atoms to that of Se atoms [9]. The structure consists of bc layers of strongly dimerized BEDT-TTF or BEDT-STF molecules, with each dimer oriented approximately perpendicular to its nearest neighbors (Supplementary Figure 2b,c).

Electrical transport was measured parallel to the c-axis from room temperature down to T=1.8 K by the standard four-probe technique. For this, thin gold wires were contacted by carbon paste. Furthermore, we measured the complex electrical impedance as a function of temperature and frequency in order to obtain the dielectric permittivity  $\hat{\varepsilon}=\varepsilon_1+\mathrm{i}\varepsilon_2$ . Here, gold wires were attached to opposite crystal surfaces and the data recorded by an impedance analyzer in the frequency range from 40 Hz to 10 MHz covering temperatures down to T=5 K. The applied ac voltage was set to 0.5 V, making sure that we operate in the Ohmic regime.

Supplementary Figure 3 displays the c-axis dc resistivity  $\rho(T)$  as a function of temperature for all samples in our substitution series from x=0 to 1. The room-temperature values increase from approximately 0.03  $\Omega$ cm for x=1 to around 0.5  $\Omega$ cm for x=0. For x=0.12 and higher the system turns metallic at low temperatures; the range of metallic conductivity below the Brinkman-Rice temperature  $T_{\rm BR}$  increases for larger substitution and exceeds  $T=300~{\rm K}$  for  $x\geq 0.44$ . For very low temperatures, the metallic properties are clearly characterized by a  $\rho(T)\propto T^2$  behavior that is the hallmark of electron-electron interaction. A detailed analysis of the Fermi-liquid properties will be provided elsewhere.

#### SUPPLEMENTARY NOTE 2: DIELECTRIC RESPONSE AS A FUNCTION OF PRESSURE

In order to give an overview on the temperature-dependent dielectric response of  $\kappa$ -(BEDT-TTF)<sub>2</sub>Cu<sub>2</sub>(CN)<sub>3</sub> in the various regimes, in Supplementary Figure 4 we plot the real part of the dielectric permittivity  $\varepsilon_1(T)$  for selected frequencies and pressures as indicated. Starting from ambient conditions, a pronounced peak dominates the temperature



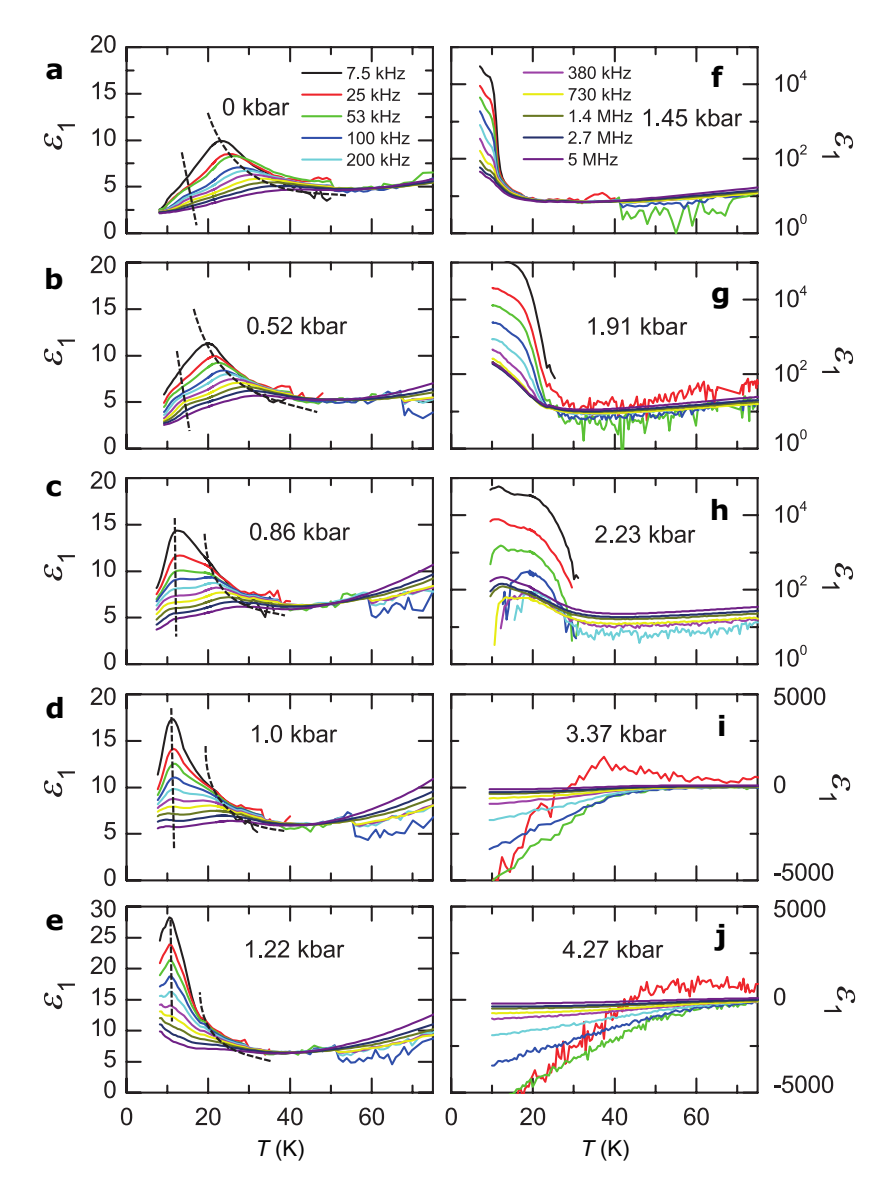
Supplementary Figure 3. Temperature dependence of the dc resistivity of  $\kappa$ -[(BEDT-STF)<sub>x</sub>(BEDT-TTF)<sub>1-x</sub>]<sub>2</sub>Cu<sub>2</sub>(CN)<sub>3</sub> for various substitution values x as indicated spanning the full range from the insulating x = 0 to the metallic side. The data are measured along the highly conducting c-axis and normalized to the respective room-temperature value for better comparison.

dependence of the dielectric constant. The maximum shifts to lower temperatures as pressure increases (Supplementary Figure 4a-e) and, exceeding p=1.22 kbar, it moves out of the accessible temperature window. Most important, however, are the drastic changes of the dielectric response around the insulator-metal transition at  $p_{\rm IMT}=1.45$  kbar [5]. For p=1.45 up to 2.2 kbar,  $\varepsilon_1$  is strongly enhanced for T<20 K with a frequency-dependent amplitude even exceeding  $10^5$  at f=7.5 kHz (Supplementary Figure 4f-h). As pressure increases further, the onset of the dielectric anomaly shifts to higher temperatures, reaching about 30 K at p=2.23 kbar, for instance (Supplementary Figure 4h). We ascribe this observation to a coexistence region centered around the Mott insulator-metal transition (IMT), where spatially segregated metallic regions in an insulating matrix grow in a percolative manner. At p=3.37 kbar and higher (Supplementary Figure 4i,j),  $\varepsilon_1$  becomes negative and large for nearly all frequencies indicating purely metallic behavior.

The most surprising observation of Supplementary Figure 4 is the dramatic increase of the dielectric constant of  $\kappa$ -(BEDT-TTF)<sub>2</sub>Cu<sub>2</sub>(CN)<sub>3</sub> for p > 1.2 kbar. In Supplementary Figure 5 we plot the pressure dependence of  $\varepsilon_1(p)$  and  $\sigma_1(p)$  as obtained for a fixed frequency of f = 100 kHz at different temperatures; Fig. 3a,b of the main paper displays a similar data set recorded at 380 kHz. A pronounced peak in the permittivity appears around 1.8 kbar followed by a drop to negative values evidencing the onset of metallic conduction. We explain this observation by percolation when the insulator-metal phase boundary is approached: metallic puddles develop within the insulating matrix and grow with increasing pressure.

At the lowest temperature, T=10 K, the peak maximum occurs at a pressure slightly above  $p_{\rm IMT}$ . This can be understood when recalling the definition of the percolation threshold as the first continuous conducting path, while the dielectric constant is integrated over the entire volume; hence the overall capacitance still increases even when some inclusions already coalesce. As seen from Supplementary Figure 5a, the peak in  $\varepsilon_1(p)$  shifts to even higher pressure values as T rises, but strongly diminishes upon heating; for T>22 K the anomaly is completely suppressed. Eventually, a simple drop in permittivity remains with a change in sign to large negative values of  $\varepsilon_1(p=4.3 \text{ kbar}) \approx -10^3 \text{ to } -10^4$ .

The enhancement of the dielectric constant is accompanied by a step-like feature in the conductivity, presented in Supplementary Figure 5b. With pressure, the metallic fraction grows; consequently  $\sigma_1(p)$  rises continuously until it saturates in the metallic phase where the pressure-dependence of the conductivity is minuscule. The inflection point corresponds to  $p_{\text{IMT}}$ , defined above by dc-resistance measurements [5]. With rising temperature, the step feature shifts to higher pressure values, smears out and becomes a more gradual increase consistent with the change from the first-order IMT to the crossover region upon heating through  $T_{\text{crit}}$ .

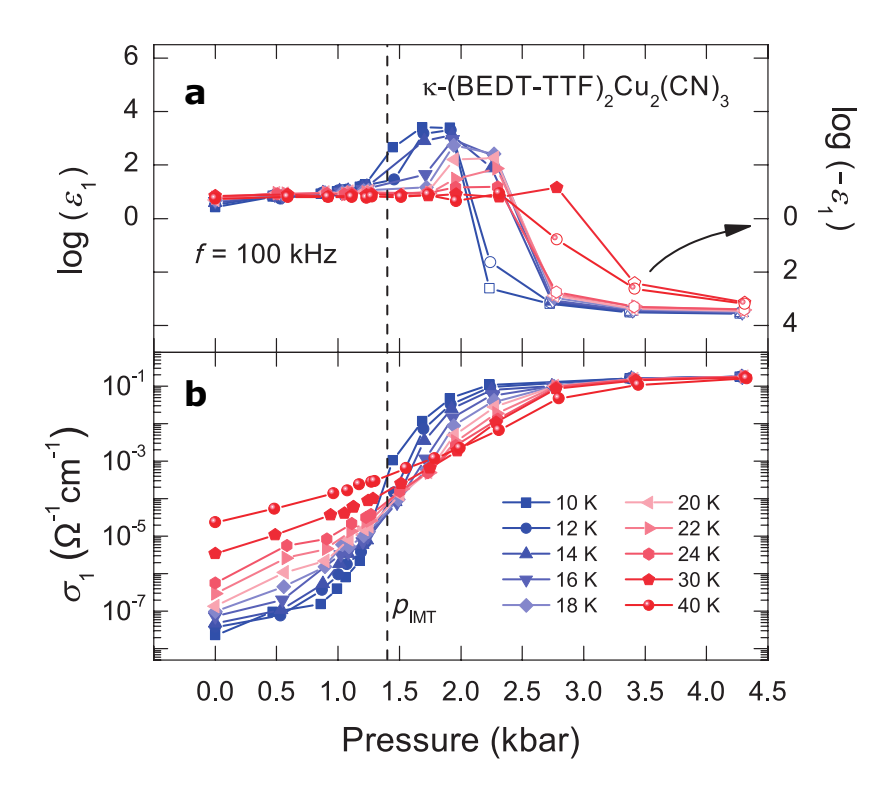


Supplementary Figure 4. Plot of the dielectric permittivity  $\varepsilon_1(T)$  of  $\kappa$ -(BEDT-TTF)<sub>2</sub>Cu<sub>2</sub>(CN)<sub>3</sub> for several frequencies from 7.5 kHz to 5 MHz upon increasing pressure. Note the different ordinates used in the various panels. **a**, At p=0 kbar and below T=50 K, we observe a relaxor-type ferroelectric peak with shrinking amplitude that shifts to higher temperature with increasing frequency. **b-e**, Additionally, a shoulder-like feature is revealed at ambient pressure around T=15 K which develops into a second peak upon pressurization. **f-h**, In the coexistence phase between p=1.45 and 2.23 kbar, an enormous increase of  $\varepsilon_1$  is observed which is strongly frequency-dependent and attributed to spatially separated metallic and insulating regions. **i,j**, Above p=3.37 kbar,  $\varepsilon_1<0$  for nearly all measured frequencies indicating metallic behavior.

The dielectric properties of percolating systems have been subject of numerous investigations for half a century [11, 12]. As pointed out by Efros and Shklovskii [13] the static dielectric constant of a percolating system is a function of the filling fraction m of the metallic phase and diverges at the percolation threshold in the limit  $T \to 0$  and  $\omega \to 0$ . The divergency gets reduced and rounded as the insulating matrix acquires a finite conductivity  $\sigma_i$ , for instance as temperature rises:

$$\varepsilon_1(T, m_c) \propto \left[ \frac{\sigma_m(T)}{\sigma_i(T)} \right]^{1-s} ,$$
(1)

where s = 0.5 and 0.62 in two and three dimensions, respectively [13], and  $\sigma_m$  denotes the conductivity of the metallic regions. Although our data do not permit a quantitative comparison, the observed reduction of the peak seen in Supplementary Figure 5a is in accord with the tendency of Eq. (1).



Supplementary Figure 5. Pressure dependence of the dielectric properties of  $\kappa$ -(BEDT-TTF)<sub>2</sub>Cu<sub>2</sub>(CN)<sub>3</sub> recorded at different temperatures for a fixed frequency f = 100 kHz. **a**, The permittivity  $\varepsilon_1$  forms a pronounced maximum followed by a rapid drop to negative values. **b**, The conductivity  $\sigma_1$  exhibits a step-like increase with an inflection point located right at the onset of the peak in  $\varepsilon_1$ . This percolating behavior stems from the nucleation and growth of metallic puddles spatially separated in an insulating matrix; the filling fraction increases by applying pressure. With rising temperature the features shift to higher pressures and diminish in amplitude and step size, respectively.

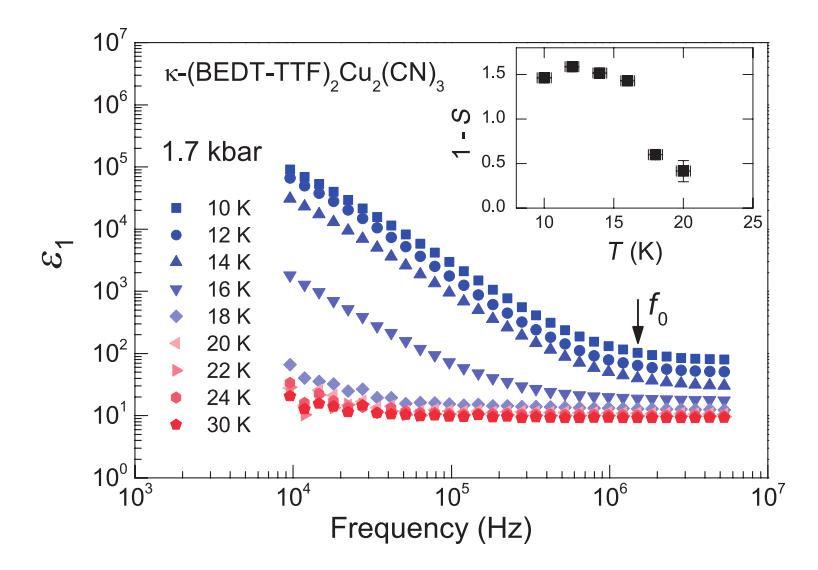
Alternatively, at T = 0 ( $\sigma_i = 0$ ) and for  $m = m_c$  one expects a reduction of the peak amplitude when probed at finite frequencies, according to [13]

$$\varepsilon_1(\omega, m_c) \propto (1/\omega)^{1-s}$$
 (2)

Choosing the pressure for which the dielectric constant reaches the maximum value, in Supplementary Figure 6 we plot the frequency-dependence of  $\varepsilon_1(\omega,p=1.7~{\rm kbar})$  for several temperatures. For  $T\leq 16~{\rm K}$ ,  $\varepsilon_1(\omega)$  strongly drops with increasing frequency following a power-law for two orders of magnitude before it levels off at  $f_0=\omega/(2\pi)\approx 2~{\rm MHz}$ . In the vicinity of the critical endpoint and above  $T_{\rm crit}$ , the percolative behavior vanishes and merges into a frequency-independent response. Following Eq. (2), we fit the data in Supplementary Figure 6 and obtain an exponent 1-s for each temperature, displayed in the inset. The deviation from theory has several reasons: standard percolation theory does not take into account field enhancement effects between adjacent finite metallic clusters beyond the dipole approximation and/or hopping of charge carriers between them as well as electron-electron interactions, as pointed out previously [14–17]. Sarychev and Brouers [18] explicitly account for tunneling between finite metallic clusters in order to explain the low-frequency response of percolating systems.

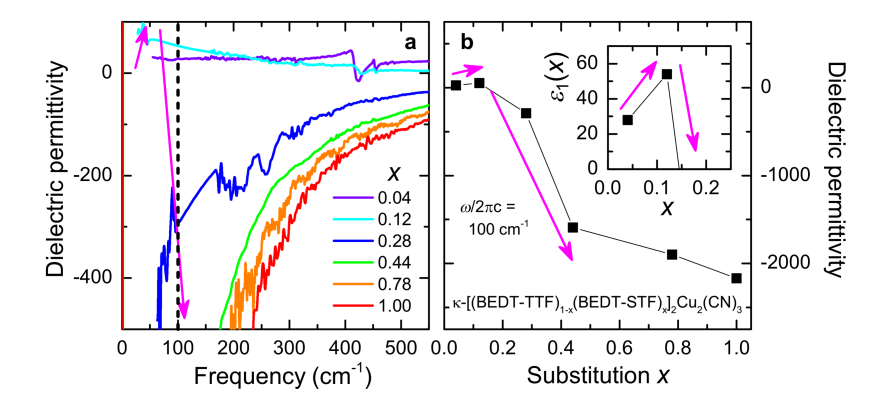
# SUPPLEMENTARY NOTE 3: DIELECTRIC RESPONSE AS A FUNCTION OF CHEMICAL SUBSTITUTION

In a first approach, the dielectric properties in the infrared spectral range can be obtained from optical reflectivity data (not shown) as a function of frequency, temperature and substitution. Supplementary Figure 7 displays the real part  $\varepsilon_1(\omega)$  for the different  $\kappa$ -[(BEDT-STF) $_x$ (BEDT-TTF) $_{1-x}$ ] $_2$ Cu $_2$ (CN) $_3$  crystals recorded at T=5 K. In the Mott-insulating state ( $x \leq 0.1$ ), the permittivity is basically frequency-independent and acquires a small, positive value. As x increases, the quasi-static  $\varepsilon_1(\omega \to 0)$  first increases before it rapidly drops to large negative values. After crossing the Mott insulator-metal transition the system becomes conductive: the strong screening of the coherent



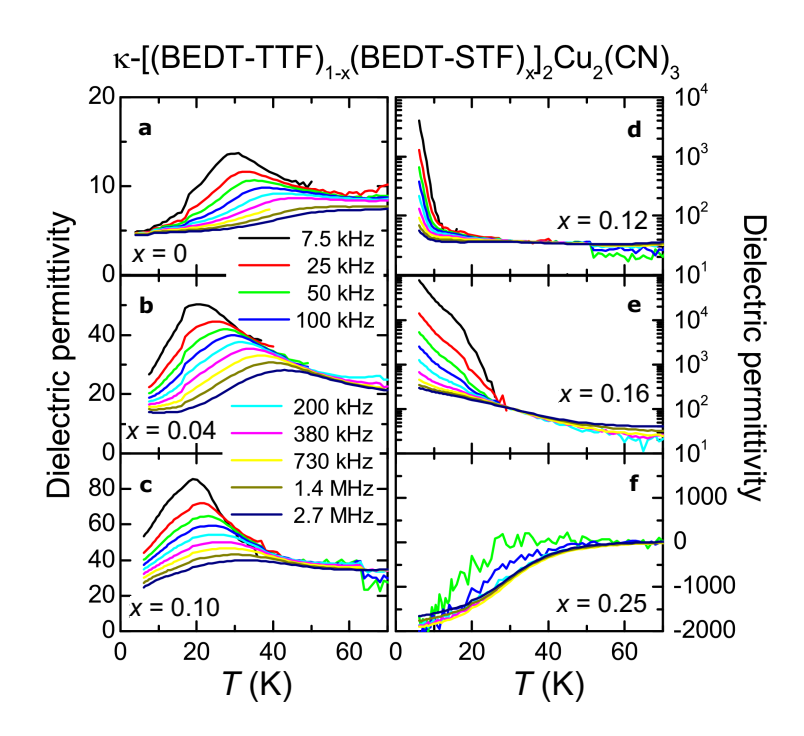
Supplementary Figure 6. Double-logarithmic plot of  $\varepsilon_1(f)$  at 1.7 kbar for various temperatures, as indicated. For  $T \leq 16$  K a power-law behavior is observed, which saturates above  $f_0 \approx 2$  MHz. The percolating behavior of  $\kappa$ -(BEDT-TTF)<sub>2</sub>Cu<sub>2</sub>(CN)<sub>3</sub> is suppressed for T > 16 K where the first-order transition becomes a gradual crossover. The inset shows the temperature dependence of the exponent 1 - s obtained from fits by Eq. (2).

quasiparticles drives  $\varepsilon_1$  negative. A similar observation was reported for the Mott transition of VO<sub>2</sub>, where the low-frequency permittivity diverges as a function of temperature. Near-field optical microscopy revealed that this behavior stems from the phase coexistence of metallic puddles in an insulating matrix [19]. In general, the divergency of the dielectric permittivity  $\varepsilon_1(x)$  is a hallmark of percolative phase transitions in microemulsions [20–24], composites [25–27] or percolating metal films [28–32].



Supplementary Figure 7. Despite continuously increasing low-frequency conductivity, in the low-frequency limit the dielectric permittivity  $\varepsilon_1(x)$  exhibits a peak around the Mott transition, reminiscent of a percolative-type coexistence of metallic and insulating regions. **a**, Real part of the dielectric permittivity  $\varepsilon_1(x)$  as obtained from far-infrared reflectivity measurements for  $E \parallel c$  at T = 5 K for  $\kappa$ -[(BEDT-STF)<sub>x</sub>(BEDT-TTF)<sub>1-x</sub>]<sub>2</sub>Cu<sub>2</sub>(CN)<sub>3</sub> with various substitutions x as indicated. **b**, To better follow the substitutional dependence, we display the dielectric permittivity taken at  $\omega/(2\pi c) = 100$  cm<sup>-1</sup> – corresponding to 3.3 THz – indicated by the dashed line in panel **a**.

Since audio- and radio-frequency experiments are more suitable for exploring the dielectric behavior at the insulator-metal transition, we have conducted dielectric experiments down to 7.5 kHz. Supplementary Figure 8 summarizes the dielectric response of  $\kappa$ -(BEDT-TTF)<sub>2</sub>Cu<sub>2</sub>(CN)<sub>3</sub> and how it is affected by moving across the Mott insulator-to-metal transition via STF-substitution. We plot the real part of the permittivity  $\varepsilon_1$  as a function of temperature T for selected frequencies f and substitutions x, as indicated. The pronounced peak dominating the temperature dependence of  $\varepsilon_1(T)$  was discovered by Abdel-Jawad *et al.* [33] and subsequently confirmed by other groups [34–37]. When probed at f = 7.5 kHz, the maximum is observed around T = 30 K in the case of  $\kappa$ -(BEDT-TTF)<sub>2</sub>Cu<sub>2</sub>(CN)<sub>3</sub> (Supplementary Figure 8a); with a slight sample-to-sample dependence, in agreement with previous reports. The peak shifts to higher



Supplementary Figure 8. Temperature-dependent dielectric permittivity of  $\kappa$ -[(BEDT-STF)<sub>x</sub>(BEDT-TTF)<sub>1-x</sub>]<sub>2</sub>Cu<sub>2</sub>(CN)<sub>3</sub> for substitutional values x = 0, 0.04, 0.10, 0.12, 0.16 and 0.25 measured at several frequencies. Note the different ordinates used in the various panels. **a,** The pure crystal exhibits a relaxor-type ferroelectric feature below T = 50 K, which becomes more pronounced and shifts to lower T as frequency gets smaller. **b,c**, As x is increased to 0.1,  $\varepsilon_1(T)$  rises strongly and the peak appears at lower temperatures. **d,e**, Eventually the permittivity reaches values of  $10^5$  due to the coexistence of spatially separated metallic and insulating regions. The response is strongly frequency dependent. **f,** Upon percolation around x = 0.2, the dielectric constant is negative, giving evidence for the metallic behavior that continues for all higher substitutions up to x = 1.

temperatures as the frequency increases; at the same time, however, it gets less pronounced. This behavior resembles the well-known phenomenology of relaxor ferroelectrics [38].

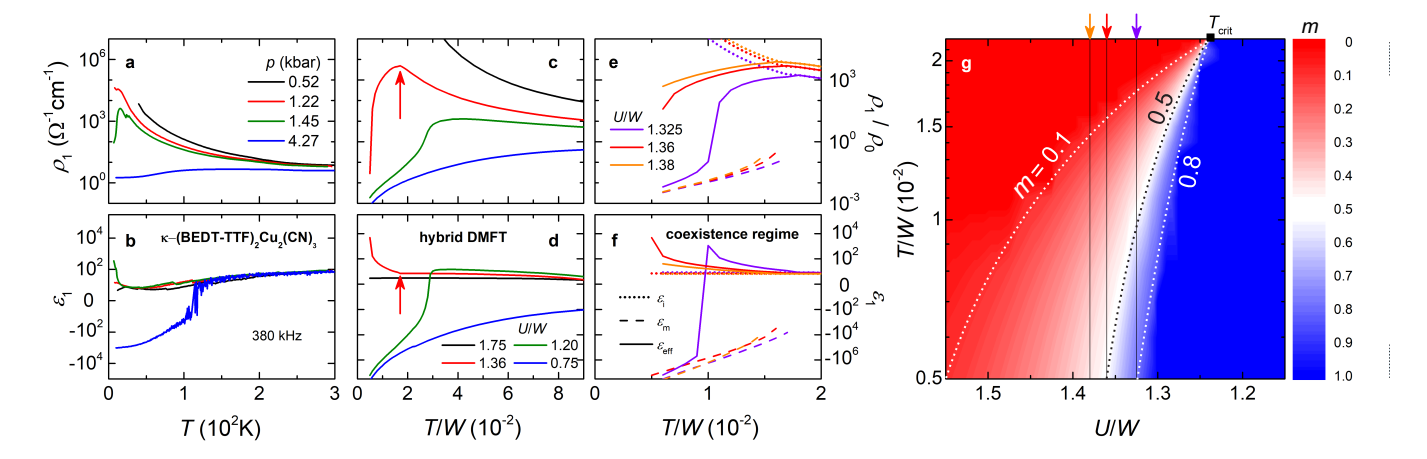
Already the minimal substitution of x=0.04 and 0.1 enhances the dielectric permittivity significantly with the maximum  $\varepsilon_1(f=7.5 \text{ kHz}) \approx 50$  and 80. This strong increase of  $\varepsilon_1(T)$  and concomitant shift of the peak to lower temperatures when we approach the insulator-metal transition is in full accord with our pressure-dependent dielectric studies in Supplementary Note 2, where an extensive and detailed analysis is given. As we approach the phase transition further (x=0.12 and 0.16), the dielectric constant drastically diverges, reaching values up to  $10^5$  in the static low-temperature limit. A divergency in  $\varepsilon_1(x)$  is the fingerprint of a percolative phase transition where metallic regions form in an insulating matrix [11, 13, 39]. When crossing the percolation threshold, the system acts like a metal, characterized by a negative dielectric permittivity,  $\varepsilon_1 < 0$ . With rising x the sign change of the dielectric constant traces the Brinkman-Rice temperature, as it was identified by the maximum in  $\rho(T)$  (Supplementary Figure 3) [40]. These results confirm the observations we extracted from the optical response in Supplementary Figure 7.

### SUPPLEMENTARY NOTE 4: THEORETICAL ANALYSIS OF THE DIELECTRIC PERMITTIVITY AT THE IMT

The dielectric properties of a mixture of spatially segregated conductive and insulating regions are commonly modelled by Bruggeman's effective medium approach [11, 41–43]:

$$m \frac{\varepsilon_m - \varepsilon_{\text{eff}}}{\varepsilon_{\text{eff}} + L(\varepsilon_m - \varepsilon_{\text{eff}})} + (1 - m) \frac{\varepsilon_i - \varepsilon_{\text{eff}}}{\varepsilon_{\text{eff}} + L(\varepsilon_i - \varepsilon_{\text{eff}})} = 0 \quad , \tag{3}$$

where m is the volume fraction of the metallic inclusions, L is the shape factor,  $\varepsilon_i$  and  $\varepsilon_{\rm m}$  are the complex permittivities of the insulating and metallic phases, respectively, and  $\varepsilon_{\rm eff}$  is the effective permittivity of the composite. In the following, we determine the complex dielectric response on purely theoretical ground. To that end, we calculate



Supplementary Figure 9. **a,b**, Pressure evolution of the temperature-dependent resistivity and permittivity measured at f=380 kHz along the a-axis of  $\kappa$ -(BEDT-TTF)<sub>2</sub>Cu<sub>2</sub>(CN)<sub>3</sub>. **c,d**, Calculated resistivity and permittivity using hybrid DMFT with different strength of effective correlations U/W as indicated. The red arrows indicate the temperature below which the coexistence regime is entered. **e,f**, For selected values of U/W close to the Mott insulator-metal transition the temperature-dependent resistivity and permittivity are plotted for the insulating phase,  $\varepsilon_i$  (dotted lines), the metallic phase  $\varepsilon_m$  (dashed lines) and the resulting effective medium  $\varepsilon_{\rm eff}$  (solid lines) at lowest temperatures in the coexistence regime. **g**, Volume fraction m of the metallic component in a false-color presentation according to the right scale. The dependence on correlation strength U and temperature U, normalized to the bandwidth U, is calculated by Eq. (6). The dotted lines represent U and U and U and U and U are U and U and U are U are U and U are U are U and U are U are U and U are U are U are U are U are U and U ar

 $\varepsilon_m(\omega, T)$  and  $\varepsilon_i(\omega, T)$  of the pure metallic and insulating phases and use them to obtain the electrodynamic properties of the mixture via Eq. (3) by utilizing a phenomenological model for the metallic filling fraction. We assume a half-filled Hubbard model in two dimensions with semicircular bands and apply dynamical mean-field theory (DMFT) calculations. Within the single site DMFT approach, the real part of optical conductivity  $\sigma_1(\omega)$  is given by the expression [44–46]

$$\sigma_{1}(\omega) = \frac{2e^{2}}{\pi\hbar} \frac{1}{a} \frac{1}{S} \int dE \, \rho_{0}(E) \left[V(E)\right]^{2}$$

$$\times \int_{-\infty}^{+\infty} d(\hbar\nu) \frac{f(\hbar\nu) - f(\hbar\nu + \hbar\omega)}{\hbar\omega}$$

$$\times \operatorname{Im} \left\{ G(\hbar\nu + \hbar\omega, E) \right\} \operatorname{Im} \left\{ G(\hbar\nu, E) \right\},$$

$$(4)$$

where

$$G\left(\hbar\nu,E\right) = \frac{1}{\hbar\nu - E - \Sigma(\hbar\nu)},$$

is the Green function and  $\Sigma(\hbar\nu)$  is the local self energy. The imaginary part of the optical conductivity  $\sigma_2(\omega)$  is then calculated via Kramers-Kronig transform [45]:

$$\sigma_2(\omega) = -\frac{2}{\pi} \int_0^\infty \frac{\omega \sigma_1(\omega')}{\omega'^2 - \omega^2} d\omega' \quad . \tag{5}$$

Applying these expressions (4) and (5), we obtain the complex dielectric response  $\hat{\varepsilon}(\omega) = 1 + i\hat{\sigma}(\omega)/(\omega\varepsilon_0)$ , via DMFT across the entire phase diagram, as a function of temperature T and the interaction U. We stress that within the coexistence region we find two locally stable solutions, while outside there is only one solution. In Eq. (4), a = 15Å, is the distance between layers for our material [1], yielding a sheet conductance  $e^2/(ha) \approx 260 \ (\Omega\text{cm})^{-1}$ .  $V(E)/\sqrt{S}$  is the current vertex, which is equal to  $\sqrt{(D^2 - E^2)/3}$ , and  $\rho_0(E) = 2\sqrt{D^2 - E^2}/\pi D^2$  is the semicircular model density of states of non-interacting electrons of bandwidth W = 2D.

In order to calculate the total dielectric function within the (percolating) coexistence region, we not only have to know the dielectric function for each of the two phases,  $\varepsilon_i$  and  $\varepsilon_m$ , but also the relative volume fraction of the

two components as a function of temperature T and effective correlations U/W. For simplicity, we use a hyperbolic tangent function to represent the metallic volume fraction m:

$$m\left(\frac{T}{W}, \frac{U}{W}\right) = \frac{1}{2} \tanh\left\{\frac{c\left[\left(U/W\right)_{\text{crit}} - \left(U/W\right)\right]}{\left(T/W\right)_{\text{crit}} - T/W}\right\} + \frac{1}{2},\tag{6}$$

which is centered around  $(U/W)_{\rm crit} = (0.20 - T/W)/0.14$ , as depicted in Supplementary Figure 9g. We also select c = 0.1 for  $U/W > (U/W)_{\rm crit}$  and c = 0.3 for  $U/W > (U/W)_{\rm crit}$  in order to mimic the experimental findings.

Finally, we obtain the optical conductivity  $\sigma_1(\omega,T)$  and dielectric permittivity  $\varepsilon_1(\omega,T)$  inside the coexistence region via the BEMA Eq. (3). We assumed  $L=\frac{1}{2}$  for our calculations, but the findings can be easily scaled to  $L=\frac{1}{3}$ . Here we focus on very low frequency  $\omega/(2\pi)=5\cdot 10^{-9}W\approx 320$  kHz, in order to allow comparison of the calculated permittivity with our experiments. For better relating our calculated to experimental results, in Supplementary Figure 9 we plot representative curves of electrical resistivity  $\rho_1(T)$  and dielectric permittivity  $\varepsilon_1(T)$  for various correlation strengths U covering the insulating, percolating and metallic regions of the phase diagram. For large U/W the system behaves insulating with a small positive dielectric constant, corresponding to the behavior observed at ambient and low pressure (p<1 kbar). For intermediate correlation strength U/W=1.36, the resistivity starts insulating at high temperatures, but  $\rho_1(T)$  exhibits a maximum around  $T/W\approx 1.6$  below which it turns weakly metallic. Upon cooling, the system enters the coexistence regime with metallic inclusions, as depicted in Supplementary Figure 9g. Around that temperature,  $\varepsilon_1(T)$  rises rapidly, acquiring  $10^4$  near the percolation threshold. This temperature dependence resembles the observations on  $\kappa$ -(BEDT-TTF)<sub>2</sub>Cu<sub>2</sub>(CN)<sub>3</sub> for p=1.45 kbar. As U/W decreases further, the phase boundary to the metallic phase is crossed with a drop in  $\rho_1(T)$  and a sign change in the dielectric constant. For U/W=1.75 metallic properties are found in the entire temperature range. This behavior is reached for the highest pressure values above 4 kbar. The full set of data is presented in Figs. 1 and 4.

Here we want to focus on the regime right at the IMT and therefore plot the behavior for U/W close to the critical correlation strength. In Supplementary Figure 9e,f the properties  $\rho_1(T)$  and  $\varepsilon_1(T)$  of the constituting insulating and metallic phases are plotted together with the effective behavior  $\varepsilon_{\rm eff}$ . The coexistence regime is entered around T/W = 0.016 to 0.018 – the particular value depends on the effective correlations U/W according to Eq. (6) – and there the resistivity drops, accompanied by a change in sign of the dielectric constant to large negative values due to screening in the metal. For U/W = 1.325 the metallic state is reached at significantly lower temperatures, as seen in Supplementary Figure 9g.

#### Supplementary References

- [1] Geiser, U. et al. Superconductivity at 2.8 K and 1.5 kbar in  $\kappa$ -(BEDT-TTF)<sub>2</sub>Cu<sub>2</sub>(CN)<sub>3</sub>: The first organic superconductor containing a polymeric copper cyanide anion. *Inorg. Chem.* **30**, 2586–2588 (1991).
- [2] Komatsu, T., Matsukawa, N., Inoue, T. & Saito, G. Realization of superconductivity at ambient pressure by band-filling control in  $\kappa$ -(BEDT-TTF)<sub>2</sub>Cu<sub>2</sub>(CN)<sub>3</sub>. J. Phys. Soc. Jpn. **65**, 1340–1354 (1996).
- [3] Keysight technologies. Impedance measurement handbook, 6 Edn. (2009).
- [4] Kurosaki, Y., Shimizu, Y., Miyagawa, K., Kanoda, K. & Saito, G. Mott transition from a spin liquid to a Fermi liquid in the spin-frustrated organic conductor  $\kappa$ -(ET)<sub>2</sub>Cu<sub>2</sub>(CN)<sub>3</sub>. Phys. Rev. Lett. **95**, 177001 (2005).
- [5] Furukawa, T., Kobashi, K., Kurosaki, Y., Miyagawa, K. & Kanoda, K. Quasi-continuous transition from a Fermi liquid to a spin liquid in  $\kappa$ -(ET)<sub>2</sub>Cu<sub>2</sub>(CN)<sub>3</sub>. Nat. Commun. 9, 307 (2018).
- [6] Rösslhuber, R., Uykur, E. & Dressel, M. Pressure cell for radio-frequency dielectric measurements at low temperatures. Rev. Sci. Instr. 89, 054708 (2018).
- [7] Pustogow, A. et al. Quantum spin liquids unveil the genuine Mott state. Nat. Mater. 17, 773-777 (2018).
- [8] Furukawa, T., Miyagawa, K., Tanigchi, H., Kato, R. & Kanoda, K. Quantum criticality of Mott transition in organic materials. *Nat. Phys.* 11, 221–224 (2015).
- [9] Saito, Y., Minamidate, T., Kawamoto, A., Matsunaga, N. & Nomura, K. Site-specific <sup>13</sup>C nmr study on the locally distorted triangular lattice of the organic conductor κ (BEDT TTF)<sub>2</sub>Cu<sub>2</sub>(CN)<sub>3</sub>. Phys. Rev. B 98, 205141 (2018).
- [10] Kandpal, H. C., Opahle, I., Zhang, Y.-Z., Jeschke, H. O. & Valentí, R. Revision of model parameters for  $\kappa$ -type charge transfer salts: An ab initio study. *Phys. Rev. Lett.* **103**, 067004 (2009).
- [11] Kirkpatrick, S. Percolation and conduction. Rev. Mod. Phys. 45, 574–588 (1973).
- [12] Shklovskii, B. I. & Efros, A. L. Electronic properties of doped semiconductors (Springer-Verlag, Berlin, 1984).
- [13] Efros, A. L. & Shklovskii, B. I. Nonmonotonic relaxation kinetics of confined systems. Phys. Stat. Sol. (b) 76, 475 (1976).
- 14] Laibowitz, R. B. & Gefen, Y. Dynamic scaling near the percolation threshold in thin Au films. *Phys. Rev. Lett.* **53**, 380–383 (1984).
- [15] Hundley, M. F. & Zettl, A. Temperature-dependent ac conductivity of thin percolation films. *Phys. Rev. B* **38**, 10290–10296 (1988).

- [16] Yoon, C. S. & Lee, S.-I. Measurements of the ac conductivity and dielectric constant in a two-dimensional lattice percolation system. Phys. Rev. B 42, 4594–4597 (1990).
- [17] Pakhomov, A. B., Wong, S. K., Yan, X. & Zhang, X. X. Low-frequency divergence of the dielectric constant in metal-insulator nanocomposites with tunneling. *Phys. Rev. B* **58**, R13375–R13378 (1998).
- [18] Sarychev, A. K. & Brouers, F. New scaling for ac properties of percolating composite materials. Phys. Rev. Lett. 73, 2895–2898 (1994).
- [19] Qazilbash, M. M. et al. Mott transition in VO<sub>2</sub> revealed by infrared spectroscopy and nano-imaging. Science 318, 1750–1753 (2007).
- [20] Grannan, D. M., Garland, J. C. & Tanner, D. B. Critical behavior of the dielectric constant of a random composite near the percolation threshold. *Phys. Rev. Lett.* **46**, 375–378 (1981).
- [21] van Dijk, M. A., Casteleijn, G., Joosten, J. G. H. & Levine, Y. K. Percolation in oil-continuous microemulsions. a dielectric study of aerosol ot/water/isooctane. J. Chem. Phys. 85, 626–631 (1986).
- [22] Clarkson, M. T. & Smedley, S. I. Electrical conductivity and permittivity measurements near the percolation transition in a microemulsion: I. experiment. *Phys. Rev. A* 37, 2070–2078 (1988).
- [23] Clarkson, M. T. Electrical conductivity and permittivity measurements near the percolation transition in a microemulsion. ii. interpretation. *Phys. Rev. A* 37, 2079–2090 (1988).
- [24] Alexandrov, Y., Kozlovich, N., Feldman, Y. & Texter, J. Dielectric spectroscopy of cosurfactant facilitated percolation in reverse microemulsions. *J. Chem. Phys.* **111**, 7023–7028 (1999).
- [25] Pecharromán, C. & Moya, J. S. Experimental evidence of a giant capacitance in insulator–conductor composites at the percolation threshold. *Adv. Mater.* **12**, 294–297 (2000).
- [26] Pecharromán, C., Esteban-Betegón, F., Bartolomé, J. F., López-Esteban, S. & Moya, J. S. New percolative batio3–ni composites with a high and frequency-independent dielectric constant ( $\varepsilon_r \approx 80000$ ). Adv. Mater. 13, 1541–1544 (2001).
- [27] Nan, C.-W., Shen, Y. & Ma, J. Physical properties of composites near percolation. Ann. Rev. Mater. Res. 40, 131–151 (2010).
- [28] Berthier, S., Peiro, J., Fagnent, S. & Gadenne, P. Infrared absorption of granular metal films in the percolation range. *Physica A* **241**, 1 5 (1997).
- [29] Hövel, M., Gompf, B. & Dressel, M. Dielectric properties of ultrathin metal films around the percolation threshold. *Phys. Rev. B* 81, 035402 (2010).
- [30] Hövel, M., Gompf, B. & Dressel, M. Electrodynamics of ultrathin gold films at the insulator-to-metal transition. *Thin Solid Films* **519**, 2955 2958 (2011).
- [31] De Zuani, S., Peterseim, T., Berrier, A., Gompf, B. & Dressel, M. Second harmonic generation enhancement at the percolation threshold. *Applied Physics Letters* **104**, 241109 (2014).
- [32] De Zuani, S. et al. Suppressed percolation in nearly closed gold films. ACS Photonics 3, 1109–1115 (2016).
- [33] Abdel-Jawad, M. et al. Anomalous dielectric response in the dimer mott insulator  $\kappa$ -(BEDT-TTF)<sub>2</sub>Cu<sub>2</sub>(CN)<sub>3</sub>. Phys. Rev. B 82, 125119 (2010).
- [34] Pinterić, M. et al. Anisotropic charge dynamics in the quantum spin-liquid candidate  $\kappa$ -(BEDT-TTF)<sub>2</sub>Cu<sub>2</sub>(CN)<sub>3</sub>. Phys. Rev. B **90**, 195139 (2014).
- [35] Pinterić, M. et al. What is the origin of anomalous dielectric response in 2d organic dimer mott insulators  $\kappa$ -(bedt-ttf)<sub>2</sub>Cu[N(CN)<sub>2</sub>]Cl and  $\kappa$ -(BEDT-TTF)<sub>2</sub>Cu<sub>2</sub>(CN)<sub>3</sub>. Physica B **460**, 202 207 (2015).
- [36] Tomić, S. & Dressel, M. Ferroelectricity in molecular solids: a review of electrodynamic properties. *Rep. Prog. Phys.* **78**, 096501 (2015).
- [37] Sasaki, S., Iguchi, S., Yoneyama, N. & Sasaki, T. X-ray irradiation effect on the dielectric charge response in the dimer–mott insulator κ-(BEDT-TTF)<sub>2</sub>Cu<sub>2</sub>(CN)<sub>3</sub>. J. Phy. Soc. Jpn. 84, 074709 (2015).
- [38] Cross, L. E. Relaxor ferroelectrics, 131–155 (Springer-Verlag, Berlin, Heidelberg, 2008).
- [39] Mott, N. Metal-insulator transitions (Taylor & Francis, 1990), 2 edn.
- [40] Pustogow, A. et al. (2020). To be published.
- [41] Stroud, D. Generalized effective-medium approach to the conductivity of an inhomogeneous material. *Phys. Rev. B* 12, 3368–3373 (1975).
- [42] Stroud, D. & Pan, F. P. Self-consistent approach to electromagnetic wave propagation in composite media: Application to model granular metals. *Phys. Rev. B* 17, 1602–1610 (1978).
- [43] Choy, T. C. Effective medium theory: Principles and applications (Oxford University Press, Oxford, 2015), 2nd ed. Edn.
- [44] Georges, A., Kotliar, G., Krauth, W. & Rozenberg, M. J. Dynamical mean-field theory of strongly correlated fermion systems and the limit of infinite dimensions. *Rev. Mod. Phys.* **68**, 13–125 (1996).
- [45] Economou, E. Green's functions in quantum physics (Springer-Verlag, Berin, 2006), 3 edn.
- [46] Letfulov, B. M. & Freericks, J. K. Dynamical mean-field theory of an Ising double-exchange model with diagonal disorder. Phys. Rev. B 64, 174409 (2001).